UCRL-10348 c.2 rpl.
UC-34 Physics Distribution
TID-4500 (17th Ed.)

UNIVERSITY OF CALIFORNIA
Lawrence Radiation Laboratory
Berkeley, California

Contract No. W-7405-eng-48

HYPERON PRODUCTION BY K^- INTERACTIONS IN DEUTERIUM

Orin Iver Dahl

(Ph. D. Thesis)

July 3, 1962

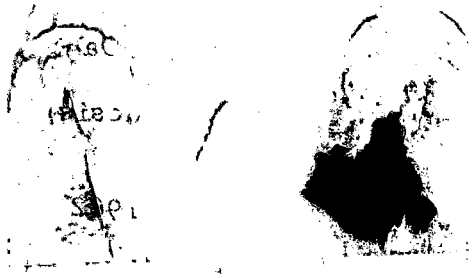

Printed in USA. Price $1.50. Available from the
Office of Technical Services
U. S. Department of Commerce
Washington 25, D.C.

DISCLAIMER

HYPERON PRODUCTION BY K^- INTERACTIONS IN DEUTERIUM

Contents

HYPERON PRODUCTION BY K^- INTERACTIONS IN DEUTERIUM

Orin Iver Dahl

Lawrence Radiation Laboratory
University of California
Berkeley, California

July 3, 1962

ABSTRACT

Hyperon production by K^- interactions in deuterium at a laboratory-system momentum of 200 MeV/c is described. The experiment was performed at the Bevatron; the Lawrence Radiation Laboratory's 15-inch deuterium bubble chamber was used.

The experimental setup and the PACKAGE-EXAMIN data-analysis system are described in the first part of the report. The separation of interactions at rest and in flight is discussed in detail.

The reactions are dominated by three-body final states. Branching ratios between the several final states provide two independent verifications of the charge-independence hypothesis. The ratios are in reasonable agreement with those predicted from the K^- p interaction. Analysis of the energy distributions in the final state indicates the presence of final-state scattering as well as a dominating impulse type of K^- nucleon interaction.

I. INTRODUCTION

In the summer of 1960 a new 800-MeV/c K^- beam was designed and built at the Bevatron. By use of the 15-inch hydrogen bubble chamber, K^- exposures were made at several momentum settings with both hydrogen and deuterium in the chamber. During part of the run, incident K^-'s were brought into the deuterium chamber in a momentum region around 200 MeV/c.

At this energy the following hyperon-producing reactions can occur.

$$K^- + d \rightarrow \begin{cases} \Lambda + \pi^- + p\,, \\ \Lambda + \pi^0 + n, \\ \Sigma^0 + \pi^- + p\,, \\ \Sigma^0 + \pi^0 + n, \\ \Sigma^- + \pi^0 + p\,, \\ \Sigma^- + \pi^+ + n, \\ \Sigma^+ + \pi^- + n, \\ \Lambda + n, \\ \Sigma^0 + n\,, \\ \Sigma^- + p\,, \text{ and} \\ \Lambda + N + 2\pi\,. \end{cases}$$

The following scattering reaction may also occur

$$K^- + d \rightarrow \begin{cases} K^- + d \\ K^- + p + n \\ \overline{K^0} + n + n\,. \end{cases}$$

We describe the hyperon-producing reactions at 200 MeV/c. Because the single-pion final states are the dominant modes, we emphasize them.

II. EXPERIMENTAL PROCEDURE

A. Beam

As the beam used in this experiment has been described elsewhere, only a brief summary is given in this report.[1] The chief problem in building a K^- beam at the Bevatron is to eliminate unwanted background particles (principally pions). In the present beam this was done by two parallel-plate electrostatic spectrometers utilizing glass cathodes.[2] These separators have crossed electric and magnetic fields that are adjusted to deflect all particles except those with the mass of K mesons.

Figure 1 shows the beam setup. The particles emerged from the Bevatron at a momentum of 800 MeV/c and were brought into paralled trajectories by the quadrupole Q_1. They then passed through the first spectrometer and were brought to a focus at S1 by the qudrupole Q_2. At this point, the deflected pions were stopped by an 18-in. lead collimator while the K mesons passed unimpeded through a 0.25-in. slit.

The particles were then deflected through an angle of 29 deg by the bending magnet. This bend eliminated a good fraction of the remaining background, since most of the unwanted particles that passed through the first slit were off momentum and hence were deflected out of the beam.

The particles then passed through a second stage of separation using quadrupoles Q_3 and Q_4 and the second separator.

After the second stage of separation the particles passed through a copper absorber to reduce their momentum to approximately 200 MeV/c at the entrance to the bubble chamber. The momentum distribution at the entrance to the bubble chamber is shown in Fig. 2.

In the chamber, approximately 60% of the tracks were K^- mesons; the rest were mostly pions and muons. During the experiment, about 12,000 K^- mesons were observed, half of which passed

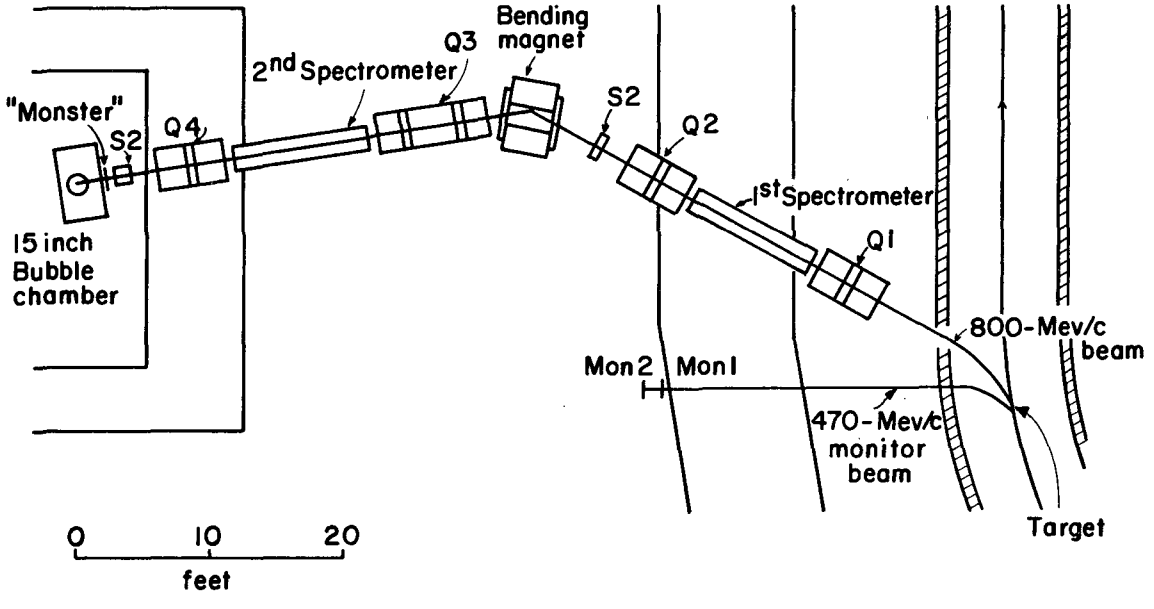

Fig. 1. Schematic diagram of the 800-MeV/c K^- beam at the Bevatron.

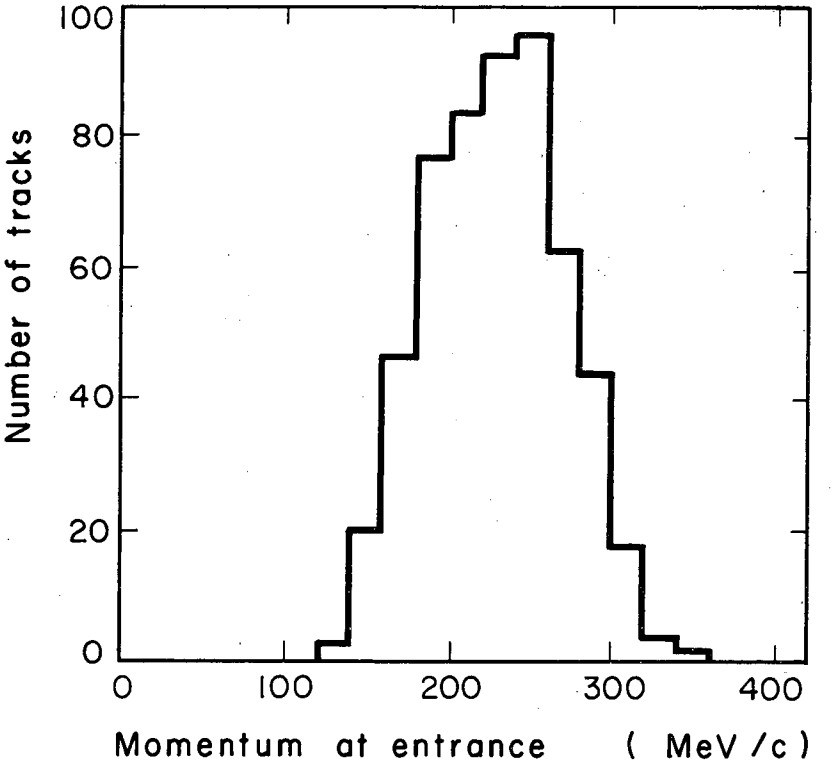

Fig. 2. Histogram of the momentum distribution, at the entrance to the chamber (551 tracks). To obtain a credible momentum measurement, only tracks with a length greater than 7 cm are plotted. Since tracks with a momentum less than 160 MeV/c would stop in less than 7 cm, the distribution cuts off sharply at this value.

through the chamber and half interacted. The total path length was 3.5 mb equivalent; i.e., we would observe 3.5 events if the cross section were exactly 1 mb. A set of four stereo photographs was taken for each bubble-chamber expansion. Approximately 10,000 such sets were taken in the whole experiment.

B. Scanning

All the film was scanned twice for K^- mesons. The K^-'s were easily distinguished from other particles because, at 200 MeV/c, they are about five times minimum-ionizing. The background pions and muons either are minimum-ionizing or else are much more curved than a K meson.

Each K meson found was recorded with a type number that specified whether the K went through the chamber or whether it interacted and, if it interacted, what type of interaction it was.

The two scans were then compared and all discrepancies were resolved. For each scan the efficiency for finding K^- interactions was approximately 95%. The resulting overall efficiency was better than 99%.

C. Sketching and Measuring

Each event of interest was then checked on a scanning table and a sketch was made of it. The sketch served to identify the tracks of the event and also to specify in which two of the four views each track was to be measured. Then the events were measured on the LRL precision-measuring projector (Franckenstein). For each track, several points on the film were measured and then punched out onto IBM cards, which were used as input for the data-processing system.

D. Data Processing

1. Event Reconstruction

After the events were measured, they were analyzed by means of the IBM 7090 program PACKAGE. PACKAGE consists of two parts, a track-reconstruction program PANG, and a kinematic analysis program KICK.[4]

The first part, PANG, reconstructs space angles and momenta from the measured points on each track. It first takes the measured points in the two views and from them constructs space points which lie along the track. The space points are then fitted to a parabola in the x-y plane and to a linear term in the z direction. Then, by use of the results of the first fit, the points are fitted to a higher-order curve that is mass-dependent and takes into account the effect of energy loss. From this second fit, space angles and momenta and their error are calculated.

2. Kinematic Fitting

KICK, the second part of PACKAGE, imposes the constraints of momentum and energy balance on the tracks at a vertex. The step serves two purposes: to reduce the uncertainties on the variables, and to distinguish between several competing hypotheses.

The analysis is done by the method of least squares. We define

$$\chi^2 = \sum_i \left(\frac{x_i^f - x_i^m}{\delta x_i} \right)^2 ,$$

where x_i^m are the measured variables, δx_i their error, and x_i^f are the adjusted values. (Actually the program includes correlated errors.) The adjusted values are selected to balance energy and momentum and to minimize the value of χ^2. The value of χ^2 is then a measure of the probability that the hypothesis is correct and may be used to resolve ambiguous cases.

The choice of variables is particularly important because, for the analysis, we assume that the input variables are Gaussian distributed. In our cases, we have chosen the azimuth angle, the slope, and the projected curvature in the x-y plane as input variables for each track.

Data on the χ^2 distribution and an examination of the errors are given in Appendix A.

3. Examination and Summary

After an event had been satisfactorily measured and fitted, it was processed by the EXAMIN system. In this stage, various useful quantities, such as angles, c.m. momenta, and effective masses, were calculated for each event and the data were summarized on convenient lists.

E. Fiducial Volume

Only events within a selected region of the chamber (fiducial volume) were selected for analysis. The chamber volume was selected with several criteria in mind; to minimize the correction due to the escape of Λ's, to accept only events in the well-illuminated region of the chamber, to get adequate momentum measurements on all charged tracks (especially the incident K^-), and to accept as large a region as possible.

III. ANALYSIS OF DATA

A. Identification of Interaction in Flight

The main difficulty in identifying the interaction in flight is that about 90% of the events in the chamber are produced by K mesons interacting at rest. Thus the interaction in flight would be badly biased by incorrectly identifying a relatively small fraction of the interaction at rest as interaction in flight.

Since in most of the final states at least one of the particles is not seen, kinematic fitting provides very little information about the momentum of the incident track. Hence, only the information on the incident track can be used to determine whether the interaction occurred at rest or in flight.

In measuring a track, the momentum information is actually measured as the projected curvature in the plane normal to the magnetic field. Then, this curvature is converted into a momentum measurement at the middle of the track and can be transformed into the momentum at the end if we use the range-momentum relation. Thus, for the incident tracks (which are flat), $1/P_{middle}$ is the momentum variable that is normally distributed.

Figures 3 and 4 show scatter plots of $1/P_{middle}$ plotted against the track length for a sample of incident beam tracks. The curves on these plots are where the points would lie if, at the end of the track, the momentum were 0, 150, or 200 MeV/c. The tracks in Fig. 3 end in a hyperon-producing interaction and are mostly produced by particles which stop. The tracks in Fig. 4 end in an elastic scattering and must be produced by particles which do not stop. From the plots it is clear that, for the scattering, the events are distributed about an average interaction momentum of 150 to 175 MeV/c, while, for the hyperon production, most of the events are distributed about an interaction momentum of 0 MeV/c with a small tail of interaction in flight in the 200-MeV/c region.

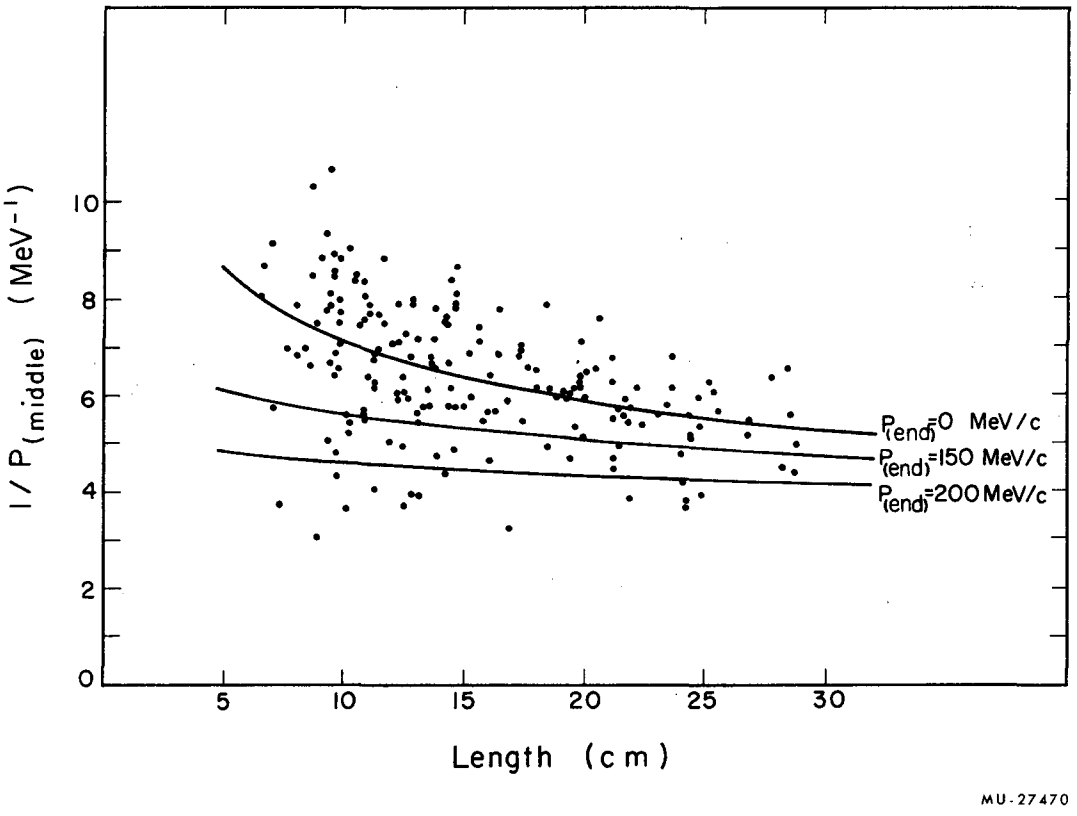

Fig. 3. Scatter plot of $(1/P_{middle})$ vs length for 180 incident K^-'s that produce hyperons. The curves show the loci of points for interaction momenta of 0, 150, and 200 MeV/c.

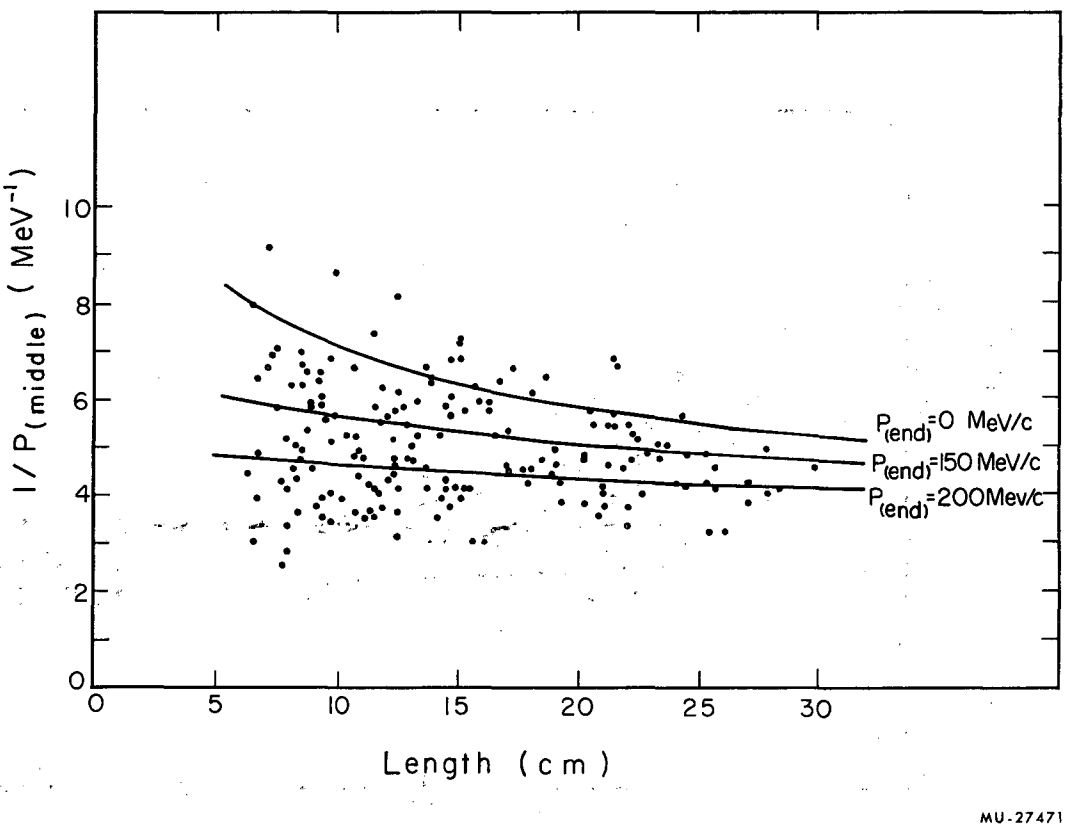

Fig. 4. Scatter plot of $(1/P_{middle})$ vs length for 175 incident K^-'s that scatter or decay. The curves show the loci of points for interaction momenta of 0, 150, and 200 MeV/c.

To determine which events were interactions in flight, the incident tracks were measured for all events that interacted in the chamber.

We chose a simple criterion to select events for further analysis. All events involving hyperons in which the incident K^- mesons had a measured momentum greater than 150 MeV/c at the end were considered to be in flight and were fully measured. Events with a measured momentum less than 150 MeV/c at the end were considered to be interactions at rest and were not measured. This selective criterion was a compromise. A higher momentum cutoff would give a slightly purer sample of interactions in flight but would reduce the number of events; a lower momentum cutoff would give a greater number of events but would introduce a larger fraction of interactions at rest into the data. It is important to minimize the number of interactions at rest since, in most cases, these events will not be eliminated by kinematic analysis but will fit as interactions in flight and remain in the data.

In one type of interaction, the events at rest and in flight can be readily separated. In the reaction

$$K^- + d \rightarrow \Lambda + \pi^- + p,$$

followed by

$$\Lambda \rightarrow \pi^- + p,$$

all the particles in the final state are seen and these events can be fitted accurately even if the incident K^- momentum is poorly measured. The results of analyzing 234 events of this type are shown in Table I.

We have divided the events into (a) interaction at rest, (b) interaction in flight at an incident momentum of less than 150 MeV/c, and (c) interaction at an incident momentum greater than 150 MeV/c. Each category has been subdivided into events in which the momentum of the incident track is measured to be less than or greater than 150 MeV/c at the interaction. We found that nearly 90% of the events are interactions at rest. Although only 3% of these interactions at rest had an incident-beam momentum measured to be greater than 150 MeV/c,

Table I. Analysis of $\Lambda\pi^-p$ events with visible proton

Measured interaction momentum	Fitted interaction momentum			Total
	< 150 MeV/c		> 150 MeV/c	
	At Rest	In Flight		
P < 150	194	11	3	208
P > 150	7	1	18	26
Total	201	12	21	234

this small fraction introduced a 25% background in the events that we considered (on the basis of the momentum measurement of the incident track) to be in flight.

B. Analysis of Events

On the scanning table the events could be separated into several classes by two criteria, (a) the topology of the interaction, and (b) identification of pions by ionization. Since the problems of analyzing and separating events in each class are different, we shall discuss each group separately.

1. The $\Sigma^0 \pi^- p$ and $\Lambda\pi^- p$ Final States

On the scanning table the unambiguous $\Sigma^0\pi^- p$ and $\Lambda\pi^- p$ events both look like V, 2-prong or V, 1-prong events; however, the two types may be separated kinematically.

To obtain a maximum amount of information about each event we have analyzed the events in which the Λ decays in the chamber via the charged mode.

On the scanning table these events may be separated into two groups:

(1) events in which the proton is seen (58 events), and

(2) events in which the proton is not seen (33 events).

In the second group of events the proton has so little energy (less than 5 MeV) that it stops before traveling far enough to produce a visible track.

In both cases the first step in the analysis was to fit the Λ decay.

Then, for the events in which the proton is visible, the two hypotheses were separated by kinematic fitting. Each event was fitted to the hypothesis $K^- + d \rightarrow \Lambda + \pi^- + p$ (4 constraints), and to the hypothesis

$$K^- + d \rightarrow \Sigma^0 + \pi^- + p;\ \Sigma^0 \rightarrow \Lambda + \gamma \text{ (2 constraints)}.$$

Then these χ^2's were used to select between the two hypotheses, thus giving an unambiguous separation for about 95% of the 91 events.

The remaining four events were assumed to be the reaction for which the χ^2 has the higher probability.

The events in which the proton was not seen were treated differently. In these events, Λ production could still be kinematically fitted, but Σ^0 production could not because three tracks were not seen. However, Λ and Σ^0 could be separated by analyzing the missing energy at the production vertex. The missing energy is

$$E_{missing} = (K_K + m_d) - (E_\Lambda + E_\pi + m_p),$$

where E is the laboratory-system energy and m is the mass of the particle specified by the subscript.

Since the proton came to rest before it had traveled far enough to make a visible track, it must have had a kinematic energy of less than 5 MeV. If the event was a $\Lambda\pi^-p$ final state, then 5 MeV is the only missing energy. However, if the event was a $\Sigma^0\pi^-p$ final state, there is also an unseen γ ray from the Σ^0 decay. This γ ray has an energy of 74 MeV in the Σ^0 rest system, but in the laboratory system its energy ranges from about 60 to 90 MeV.

Figure 5 shows the missing-energy distribution for all $\Sigma^0\pi^-p$ and $\Lambda\pi^-p$ events with no visible proton. The events are distinctly separated into two groups, one peaking around 0 to 10 MeV and the other peaking around 70 to 80 MeV. The events in the lower energy peak are $\Lambda\pi^-p$ events and those in the upper peak are $\Sigma^0\pi^-p$ events.

After the separation had been made, the $\Lambda\pi^-p$ events were kinematically fitted so that we could obtain better values for the measured variables and calculate the unmeasured variables. We analyzed the $\Sigma^0\pi^-p$ events by assuming the proton had zero kinetic energy; then we calculated the Σ^0 energy by using conservation of energy and the measurements of the K^- and π^- mesons.

In the analysis of these events we used conservation of energy rather than conservation of momentum. Since the photon has zero rest mass, its momentum and energy are equal. However, the missing

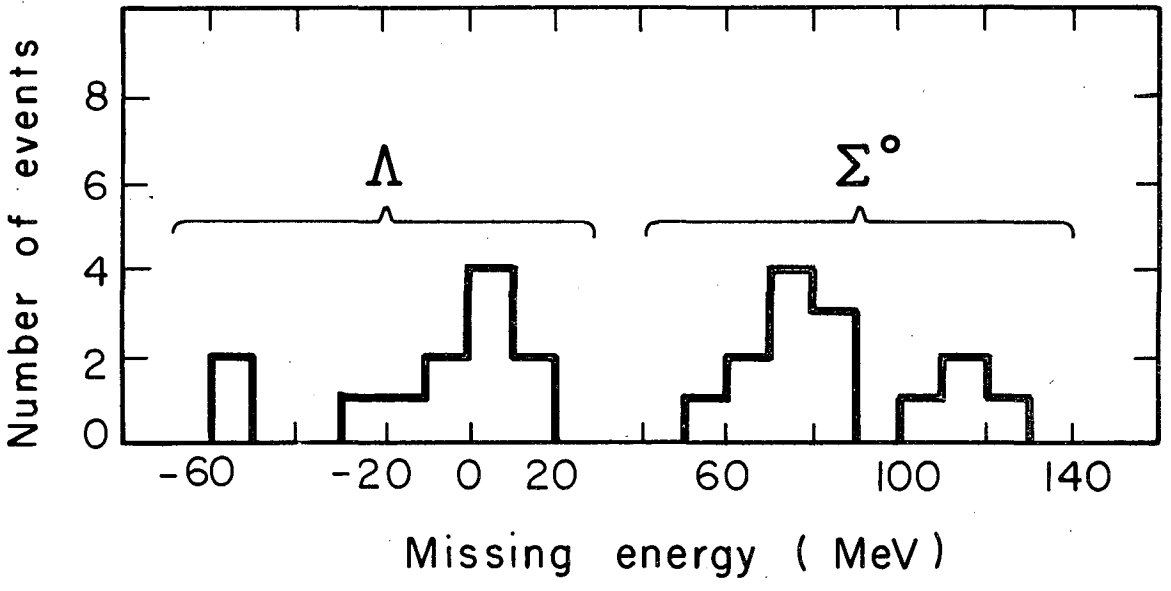

MU-27472

Fig. 5. Histogram of the distribution of missing energy in the interactions $K^- + d \rightarrow \Lambda + \pi^- + p$ and $K^- + d \rightarrow \Sigma^0 + \pi^- + p$; $\Sigma^0 \rightarrow \Lambda + \gamma$ where the proton track is invisible. The missing energy is defined as $E_m = (E_K + m_d) - (E_\Lambda + E_\pi + m_p)$.

proton is nonrelativistic and hence, whereas it has approximately 100 MeV/c maximum momentum, its kinetic energy is less than 5 MeV. Thus, although the proton momentum is equal to or larger than the momentum of the γ ray, its energy is much less and may be neglected.

2. The $\Sigma^-\pi^+n$ and $\Sigma^+\pi^-n$ Final States

Both the $\Sigma^-\pi^+n$ and the $\Sigma^+\pi^-n$ final states are easy to identify and to analyze.

The $\Sigma^-\pi^+n$ events can be identified by the presence of the π^+ in the production. At the end of its track, the Σ^- does one of two things. It (a) decays via $\Sigma^- \rightarrow \pi^- + n$ (68 events), or it (b) interacts to form a Λ and neutral particles (4 events) (the Λ may be produced directly or through the decay of a Σ^0).

In almost all cases the Σ was too short for us to measure its curvature to determine its momentum.

For the events in which the Σ decayed, the production and decay were fitted together and all the missing quantities calculated. Although measurements of the decay alone would often give a twofold ambiguity in the Σ momentum, in every case this was resolved by the production kinematics.

Since the Σ^-'s were produced with low energy, they had very little path length in which to interact before either coming to rest in the deuterium or decaying. Hence, all the Σ^- interactions were assumed to take place with the Σ at rest. The momentum of the Σ was then computed from its track length and used in fitting the production.

The Σ^+ events are also easy to identify. They can decay into either a π^+ and a neutron or a π^0 and a proton. The two decay modes can readily be distinguished, both by ionization and by kinematical analysis. These events were fitted in exactly the same way as the $\Sigma^-\pi^+n$ events in which the Σ^- decayed.

One source of ambiguity in identifying these events comes from short Σ tracks. An event that appears to be an incident K^- producing

a π^+ and a π^- can be either a Σ^- with a short track, or a Σ^+ with a short track that decays via the pionic mode. However, these events cannot be confused with any other reaction and can be separated statistically.

The biases are somewhat larger for the $\Sigma^+ \rightarrow p + \pi^0$ events because the protons have the same ionization as the Σ and, in the laboratory system, are usually emitted at small angles. These biases are more directly connected with Σ decay than with Σ production and are unimportant in an analysis of the production distribution.

3. The $\Sigma^-\pi^0 p$ Final State

The $\Sigma^-\pi^0 p$ events are experimentally the most difficult events to analyze. Since both K^-'s and Σ's are heavily ionizing these events are readily confused with K^- scatterings in which the outbound K^- either decays or interacts to form a Λ and other neutral particles.

All those events that appeared on the scanning table to be $\Sigma^-\pi^0 p$ events were measured and fitted to three hypotheses,

$$\text{(a)} \quad K^- + d \rightarrow K^- + d,$$

$$\text{(b)} \quad K^- + d \rightarrow K^- + p + n,$$

and

$$\text{(c)} \quad K^- + d \rightarrow \Sigma^- + \pi^0 + p\,.$$

The events that were elastic scatterings could then be distinguished, but in several cases the events were still ambiguous between Σ^- production and inelastic scattering. This ambiguity is reflected in the large uncertainty in the number of $\Sigma^-\pi^0 p$ events.

4. The $\Lambda\pi^0 n$ and $\Sigma^0\pi^0 n$ Final States

In the two reactions

$$K^- + d \rightarrow \Lambda + \pi^0 n$$

and

$$K^- + d \rightarrow \Sigma^0 + \pi^0 + n, \quad \text{followed by} \quad \Sigma^0 \rightarrow \Lambda + \gamma\,,$$

the only particle that can be observed is the Λ. Since, in each case, there are two unseen particles at the production, and the kinematically allowed regions of Λ momentum are approximately the same, the

two classes of events cannot be separated. Hence, in the analysis of the data, these two reactions were lumped together.

To determine the Λ momentum the decays were kinematically fitted. No fit was possible at the production vertex, since at least two particles were missing.

5. Nonmesonic Interactions

There are three possible hyperon-producing reactions that do not involve pions,

$$K^- + d \rightarrow \begin{cases} \Sigma^- + p \\ \Sigma^0 + n \\ \Lambda + n \,. \end{cases}$$

On the scanning table these reactions look like the corresponding reaction with an additional π^0, but they may be identified after analysis because the particle in the final state has a very high momentum.

In the experiment there are two events which are $K^- + d \rightarrow \Sigma^0 + n$, one event which fits $K^- + d \rightarrow \Lambda + n$, and no events of the type $K^- + d \rightarrow \Sigma^- + p$.

Of course, only 2/3 of the neutral events are observed since 1/3 of the Λ's decay via their neutral mode.

6. Multipion Events

The reaction $K^- + d \rightarrow \Lambda + 2\pi + N$ may also be observed in the experiment, but would be expected to be relatively rare because of the small amount of energy available in the final state. There are actually three possible final states of this type:

$$K^- + d \rightarrow \begin{cases} \Lambda + \pi^- + \pi^0 + p \,, \\ \Lambda + \pi^- + \pi^+ + n \,, \quad \text{and} \\ \Lambda + \pi^0 + \pi^0 + n \,. \end{cases}$$

The first reaction, $\Lambda\pi^-\pi^0 p$, looks like a $\Lambda\pi^- p$ or a $\Sigma^0\pi^- p$ event on the scanning table, but the events can be separated kinematically if the proton is visible, or they can be separated by an analysis of the missing energy in the production if the proton is not visible. The second reaction, $\Lambda\pi^-\pi^+ n$, is easily identified on the scanning table, since the positive track is lightly ionizing. The third reaction, $\Lambda\pi^0\pi^0 n$ cannot be separated from the $\Sigma^0\pi^0 n$ and $\Lambda\pi^0 n$ final states.

In the experiment there is one example of the reaction

$$K^- + d \rightarrow \Lambda + \pi^- + \pi^+ + n,$$

and none of the reaction

$$K^- + d \rightarrow \Lambda + \pi^- + \pi^0 + p .$$

C. Hyperon Branching Ratios

In estimating branching ratios for the production of the different final states we considered two sources of systematic error.

(1) In several final states, events will be ambiguous. In the reactions

$$K^- + d \rightarrow \begin{cases} \Sigma^- + \pi^+ + n, & \text{where } \Sigma^- \rightarrow \pi^- + n, \text{ and} \\ \Sigma^+ + \pi^- + n, & \text{where } \Sigma^+ \rightarrow \pi^+ + n , \end{cases}$$

there were 14 events with Σ tracks too short to be seen. These events were statistically separated by the use of the observed $\Sigma^-\pi^+ n/\Sigma^+\pi^- n$ production ratio. The $\Sigma^+ \rightarrow \pi^0 + p$ decay mode was corrected by comparing it to the $\Sigma^+ \rightarrow \pi^+ + n$ mode. We assumed that the same fraction of short-track sigmas would be missed in both cases.

To estimate the number of events in which the decay angle between the Σ^+ and the proton was too small to be seen, we looked at the projected angles between the Σ^+ and the neutron in the pionic-decay mode. Since the kinematics for the two reactions are the same, the neutron distribution should be the same as the proton distribution. We estimate that eight events were missed because the Σ^+ was short

and eight events were missed because of a small-angle decay. These missed events look like $\Lambda\pi^-p$ or $\Sigma^0\pi^-p$ final states where the Λ decays via its neutral mode.

(2) Some of the interactions are actually interactions in which the K^- meson is at rest. The only events for which we can separate interactions at rest and in flight are the $\Lambda\pi^-p$ final states that have visible protons. In these events, 30% of the events identified as interactions in flight are actually interactions at rest. We then used this number and the branching ratios for K^- interactions at rest in deuterium to estimate the number of stopping events in the other channels.[5] The total number of events observed in each final state (after correction in the Σ channels), the estimated number of these that are actually interactions at rest, and the number of events in flight are summarized in Table II.

D. Cross Sections and Path Length

For all tracks that ineracted, the path length was determined by direct measurement of the lengths of tracks in the fiducial volume. For the through tracks the path length was estimated by measurement of 10% of the tracks.

Since only events with incident K^- momenta greater than 150 MeV/c were considered in the analysis, we did not wish to include path length when the K^- was below 150 MeV/c. In the calculation of the path length, each hyperon production was assumed to be at rest and the length of track for which the K^- was below a momentum of 150 MeV/c (6.38 cm) was not counted in the path length. This gave a path length of 80,000 cm in the fiducial volume.

The cross section is defined by the relation

$$\sigma = \frac{N}{\ell \rho_A}, \quad \rho_A = \rho \frac{N_0}{A},$$

where

σ = cross section,

N = number of interactions,

ℓ = length of observed K track,

ρ_A = number of deuterons per unit volume,

Table II. Summary of cross sections for hyperon production.

Final state	Number of events observed	Estimated number of stopping events	Number of events in flight	Branching ratio	Cross section (mb)
$\Sigma^- \pi^+ n$	72	22	50±10	0.14	15±3
$\Sigma^+ \pi^- n$	96	21	75±11	0.22	23±3
$\Sigma^- \pi^0 p$	38	4	34±13	0.10	10±4
$\Sigma^0 \pi^- p$	52	4	48±8	0.14	14±2
$\Lambda \pi^- p$	85	24	61±8	0.18	18±2
$\Sigma^0 \pi^0 n$ + $\Lambda \pi^0 n$	107	33	74±12	0.21	22±3
$\Sigma^0 n$	3		3	0.009	0.09
Λn	1.5		1.5	0.004	0.05
$\Sigma^- p$	0		0		
$\Lambda \pi^- \pi^+ n$	1.5		1.5	0.004	0.05
$\Lambda \pi^- \pi^0 p$	0		0		
Total hyperon production	405	108	347±26	1.00	115±12

ρ = density of liquid deuterium,

N_0 = Avogadro's number, and

A = atomic weight of deuterium.

The density of liquid deuterium was calculated by use of the measured density of liquid hydrogen[6] (0.0586 g/cm^3) and the relation, density of electrons in deuterium = 1.069×density of electrons in hydrogen.[7] This gives a total cross section for hyperon production as σ (hyperon production = 115±12 mb.

The cross sections for productions of each final state are shown in Table II. Essentially, all the error is from estimating the number of interactions. The other factors are relatively well measured.

E. Polarizations and Decay Asymmetries

In general, the distribution for the two-body decay of a hyperon may be expressed in its c.m. system as

$$f(\cos\theta) = \frac{1+\alpha P\cos\theta}{2},$$

where

α is the decay-asmmetry parameter,

P is the hyperon polarization, and

θ is the angle between the decay pion and the hyperon polarization.

We have calculated αP by the relation

$$\alpha P = \frac{3}{N}\sum_i \cos\theta_i \pm\sqrt{\frac{3-(\alpha P)^2}{N}}$$

for two possible directions of polarization in the c.m. system,

(a) the normal $\vec{P}_K\times\vec{P}_Y$,

and

(b) the normal $\vec{P}_N\times\vec{P}_Y$,

where $\vec{P}_K$, $\vec{P}_Y$, and $\vec{P}_N$ are the K, hyperon, and nucleon momenta at the production.

The polarizations for the several reactions are listed in Table III.

All the values of αP are consistent with zero. This is what we would expect, for we need interferences between two states to produce any polarization, and at this low energy we would expect the reactions

Table III. The observed hyperon decay asymmetries.

Reaction	Values of $\alpha \vec{P}$ (a) Production plane is $\vec{P}_K \times \vec{P}_Y$	Values of $\alpha \vec{P}$ (b) Production plane is $\vec{P}_N \times \vec{P}_Y$
$K^- + d \rightarrow \Sigma^- + \pi^+ + n$, $\Sigma^- \rightarrow \pi^- + n$	+0.17±0.23	-0.08±0.23
$\rightarrow \Sigma^+ + \pi^- + n$, $\Sigma^+ \rightarrow \pi^+ + n$	+0.38±0.26	+0.03±0.27
$\rightarrow \Sigma^+ + \pi^- + n$, $\Sigma^+ \rightarrow \pi^0 + p$	-0.06±0.41	-0.14±0.41
$\rightarrow \Sigma^- + \pi^0 + p$, $\Sigma^- \rightarrow \pi^- + n$	-0.11±0.45	+0.46±0.55
$\rightarrow \Lambda + \pi^- + p$, $\Lambda \rightarrow \pi^- + p$	-0.13±0.29	+0.07±0.29
$\rightarrow \Sigma^0 + \pi^- + p$, $\Sigma^0 \rightarrow \Lambda + \gamma$, $\Lambda \rightarrow \pi^- + p$	-0.25±0.32	+0.35±0.32
$\rightarrow \left\{ \begin{array}{l} \Sigma^0 + \pi^0 + n,\ \Sigma^0 \rightarrow \Lambda + \gamma,\ \Lambda \rightarrow \pi^- + p \\ \Lambda + \pi^0 + n,\ \Lambda \rightarrow \pi^- + p \end{array} \right\}$	+0.17±0.22	

The value of αP has been calculated for two different production planes in the c.m. system: (a) the K-hyperon plane, and (b) the plane formed by the three-body final state.

to be pure S wave. Of course, for the pionic decay mode of the Σ^- and Σ^+ we would not expect any asymmetry, since α is small.

F. Representation of Data

We plotted the data in two ways:

(1) The variables in the final state can conveniently be displayed on a Dalitz plot.[8] Because the energy at which the interaction takes place is not constant, we have plotted normalized kinetic energies for the pion and the nucleon. They are defined as

$$T_{norm} = T \cdot \frac{Q_{200}}{Q},$$

where

T_{norm} = normalized kinetic energy,

T = kinetic energy in c.m. system,

Q = total kinetic energy for all three particles,

and

Q_{200} = total kinetic energy for all three particles at an incident K^- momentum of 200 MeV/c (this is a constant for each final state).

The plots of normalized kinetic energy remove most of the spread of the Dalitz plots caused by different total energies.

(2) The dominance of the impulse model can best be shown by a plot of the nucleon kinetic energy in the laboratory system. This plot can then be compared directly with the deuteron wave function.

IV. DISCUSSION OF RESULTS

A. Charge Independence

The interaction of K^- mesons in deuterium is a good place for one to check the validity of charge independence for interactions involving strange particles. The advantage of using K^- interactions in deuterium is that since the deuteron has $I = 0$, the initial state is a pure isotopic-spin state.

We shall consider interactions of the type $K^- + d \rightarrow \pi + Y + N$, where $Y = \Sigma$ or Λ. If isotopic spin is conserved, we may express the rates for the production of the various final states in terms of matrix elements for the production of any pair of particles in a pure isotopic-spin state. There are then three independent matrix elements necessary to describe the interaction. We choose M_0 and M_1 (the matrix elements for production of Σ-π in $I = 0$ and in $I = 1$) and M_Λ (the matrix element for production of Λ-π). When we calculate rates these three amplitudes and the relative phase between the $I = 0$ and $I = 1$ amplitudes for Σ-π production have physical significance. Thus, we may describe the production rates in terms of four parameters, as shown in Table IV.

Because there are seven different reactions we have three identities which must be satisfied if charge independence is correct. As we may see from Table IV, they are

$$\text{number of } \Lambda\pi^-p = 2\times \text{number of } \Lambda\pi^0n,$$

$$\text{number of } \Sigma^0\pi^-p = \text{number of } \Sigma^-\pi^0p,$$

and

$$\text{number of charged pions} = 2\times \text{number of neutral pions}.$$

Since, in this experiment, we cannot separate the $\Sigma^0\pi^0n$ events from the $\Lambda\pi^0n$ events, we cannot check the first identity.

For the other two identities we get

$$\frac{\text{number of charged pions}}{\text{number of neutral pions}} = 2.16\pm0.18,$$

and

$$\frac{\text{number of } \Sigma^-\pi^0p}{\text{number of } \Sigma^0\pi^-p} = 0.71\pm0.28.$$

Table IV. K^--d branching ratios calculated by use of charge independence.

Final state	Matrix element	Observed number of events	Adjusted values satisfying charge independence	
			Number of events	Branching ratio
$\Sigma^- \pi^+ n$	$\left\|\frac{1}{\sqrt{3}} M_0 - \frac{1}{\sqrt{6}} M_1\right\|^2$	50±10	51	0.15
$\Sigma^+ \pi^- n$	$\left\|\frac{1}{\sqrt{3}} M_0 + \frac{1}{\sqrt{6}} M_1\right\|^2$	75±11	76	0.22
$\Sigma^- \pi^0 p$	$\frac{1}{3} M_1^2$	34±13	44	0.13
$\Sigma^0 \pi^- p$	$\frac{1}{3} M_1^2$	48±8	44	0.13
$\Lambda \pi^- p$	$\frac{2}{3} M_\Lambda^2$	61±8	61	0.18
$\Sigma^0 \pi^0 n$	$\frac{1}{3} M_0^2$	74±12[a]	41	0.12
$\Lambda \pi^0 n$	$\frac{1}{3} M_\Lambda^2$		31	0.09

[a] Total events for both states.

Both ratios are in agreement with the predictions of charge independence. The value of the second ratio, however, is statistically not very significant.

We may also compute a χ^2 for the fit to charge independence. We define

$$\chi^2 = \sum_{i=1}^{6} \left(\frac{N_i^f - N_i^m}{\delta N_i} \right)^2 ,$$

where

N_i^m are the measured number of events,

δN_i are the measured uncertainties,

and

N_i^f are adjusted values.

Here we combine the $\Sigma^0\pi^0 n$ and $\Lambda\pi^0 n$ events. We then pick the values of N_i^f that satisfy charge independence and give a minimum value of χ^2. These fitted values are shown in Table IV. We get $\chi^2 = 1.05$ with two constraints. This is an excellent fit to the data, since the probability of getting a higher value of χ^2 is 65%.

In this system, we would expect deviations from charge independence to be primarily caused by two effects in the initial state. (Dalitz and Tuan have emphasized this in their study of the $K^- p$ system[18]),

(a) Coulomb scattering in the K^-d system, and

(b) kinematic effects due to the $K^- - K^0$ mass difference.

We may estimate the magnitudes of these effects and compare them with the kinetic energy available in the initial state.

We can crudely estimate the energy in the Coulomb interaction by

$$E_C = e^2 / r.$$

The appropriate radius here is the wave number of the incident K^-, $\frac{\hbar}{P_K}$; that is we "average" over the wave packet. Thus we get $E_C \approx aP_K \approx 1$ MeV ($P_K \approx 200$ MeV). The $K^- - K^0$ mass difference is

approximately 4 MeV. However, since in this experiment the incident K^- has a kinetic energy of approximately 30 MeV, both effects will probably be small.

B. The Reaction $K^- + d \rightarrow \Lambda + \pi^- + p$

In the $\Lambda\pi^- p$ final states, the outstanding feature of the Dalitz plot (Fig. 6) is that it is not uniformly populated. The events are concentrated in two regions.

(1) There is a large group of events with $T_p < 10$ MeV.

(2) There is a band of events with $T_\pi \approx 115$ MeV.

The events with low proton momentum are a consequence of the loose structure of the deuteron. These events are from K^- interactions on a single nucleon. The reaction is essentially $K^- + n \rightarrow \Lambda + \pi^-$, and the proton merely participates as a spectator.

For this type of interaction we would expect the proton-energy distribution to be simply the Fourier transform of the deuteron wave function.

Figure 7 shows the laboratory-system kinetic-energy distribution of the 37 measured events.

For the curve on the figure we have used the Hulthèn wave function $(e^{-\alpha r} - e^{-\beta r})/r$, where $\alpha = 45$ MeV and $\beta = 6.3\alpha$.

About 60% of the events fit the impulse model and the rest form a flat background. The latter are mostly events from the group with $T_\pi = 115$ MeV.

This second group of events occurs at a pion energy typical for Σ production ($T_\pi = 115$ MeV). These events suggest that a two-step process is taking place.

The primary interaction is $K^- + N \rightarrow \Sigma + \pi^-$, where the other nucleon is simply a spectator. Then the Σ interacts with this nucleon to form a Λ via the reaction $\Sigma + N \rightarrow \Lambda + N$. This process has been analyzed in detail by Karplus and Rodberg[9] and by Kotani and Ross.[10]

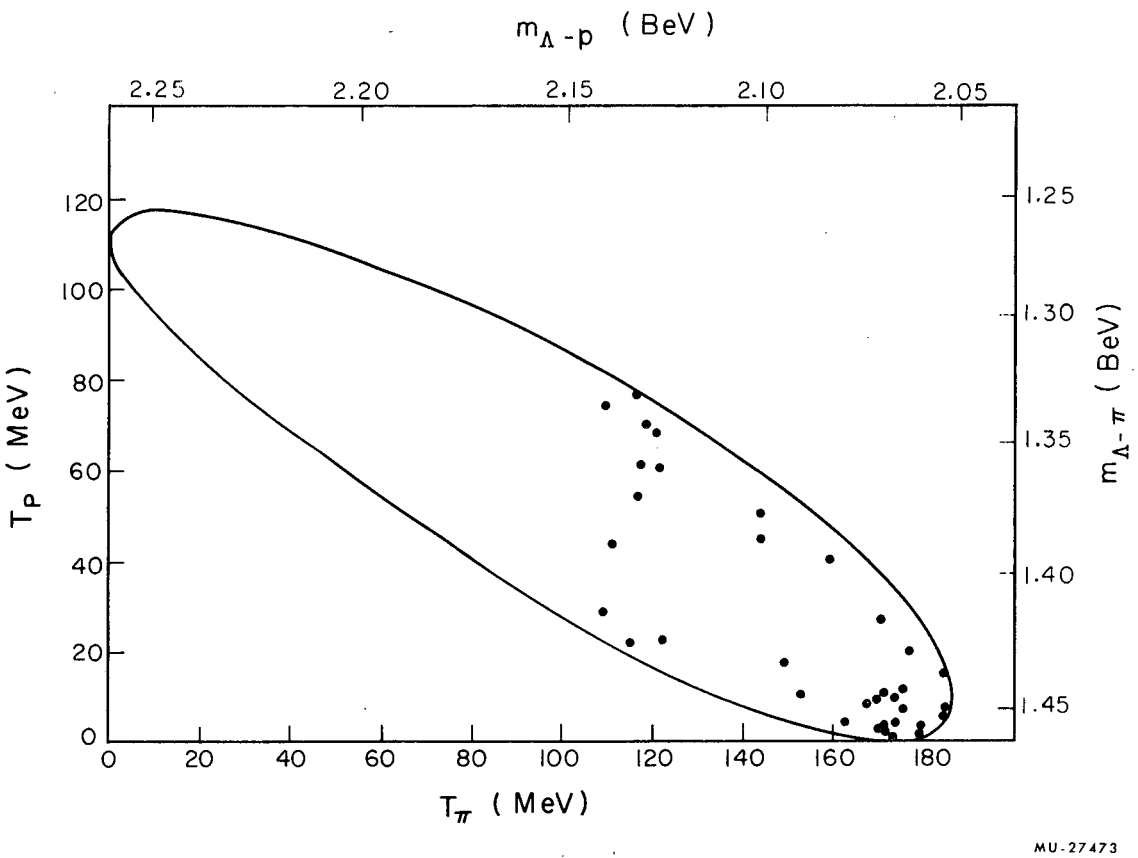

Fig. 6. Dalitz plot for the reaction
$K^- + d \rightarrow \Lambda + \pi^- + p$.

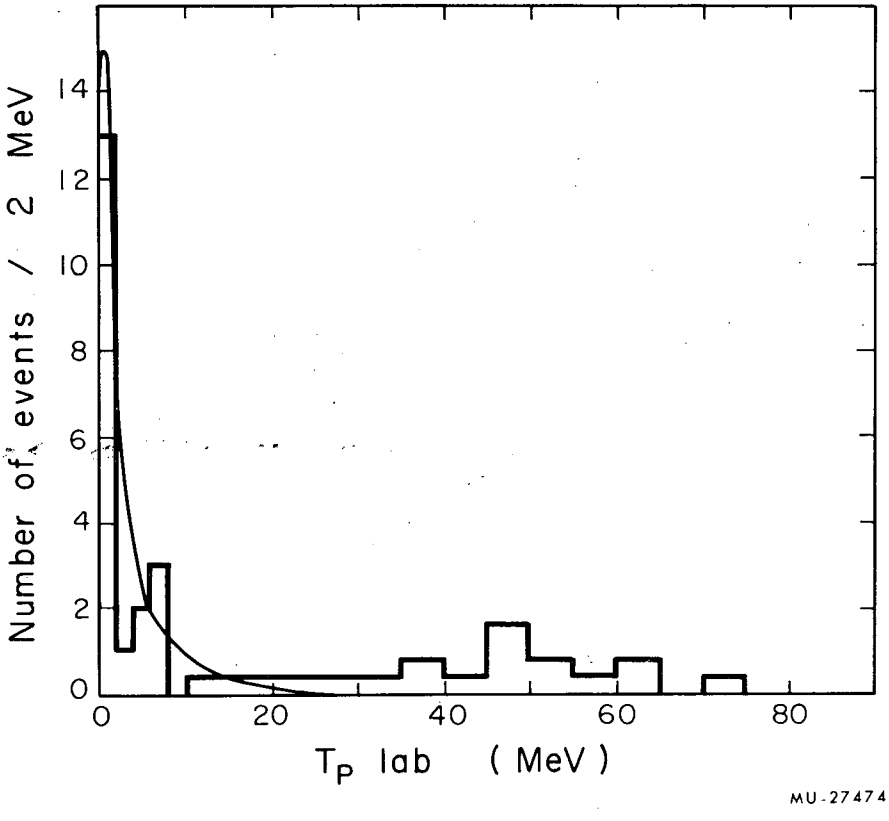

Fig. 7. Histogram of the laboratory-system energy of the proton in the reaction $K^- + d \rightarrow \Lambda + \pi^- + p$. The curve is the prediction of the impulse model.

The pion-nucleon scattering is not important at 115 MeV because, since the deuteron has zero I spin, the π-N system is in a pure $I = 1/2$ state.

In Fig. 8 we plotted the distribution of the pion kinetic energy in the c.m. system. Since the pion kinetic energy for Σ production increases as the incident energy is increased, we have normalized all the energies to an incident-beam momentum of 200 MeV/c. Although the data are clearly insufficient for a detailed comparison with theory, the observed conversions are readily accounted for by a reasonable choice of parameters in the zero-effective-range S-wave theory.

In Fig. 8, the curve for the conversion is calculated for K^- d interactions in flight by use of a slight extension of Karplus and Rodberg's S-wave formulas. For the Σ-N scattering length we have used $A_0\ B_0 = (-1+i)f$,† the same value that Miller et al. used in analyzing $K^- + d \rightarrow \Lambda + \pi^- + p$ when the K^- stops.[11]

In an analysis of this reaction at rest, Miller et al. found that it was produced by three different mechanisms:[11]

(a) direct K^--nucleon impulse-type interaction (31%),

(b) final-state internal conversion (36%), and

(c) production and decay of the 1380-MeV $\Lambda\pi$ resonance (33%).

To look for Y_1^* production we have plotted the distribution of the square of the effective mass of the Λ-π system in Fig. 9. This distribution will be roughly flat if the reaction follows phase-space predictions. The peaking between 2.05 and 2.15 $(BeV)^2$ is simply a reflection of the impulse model, since, for these events, the proton has low energy and thus the Λ-π system has high energy. In this plot we see no evidence for Y_1^*(1380 MeV) production and can say that less than two events represent this mode.

---

† Note that Karplus and Rodberg use the convention that a negative real part corresponds to an attractive potential with no bound state.

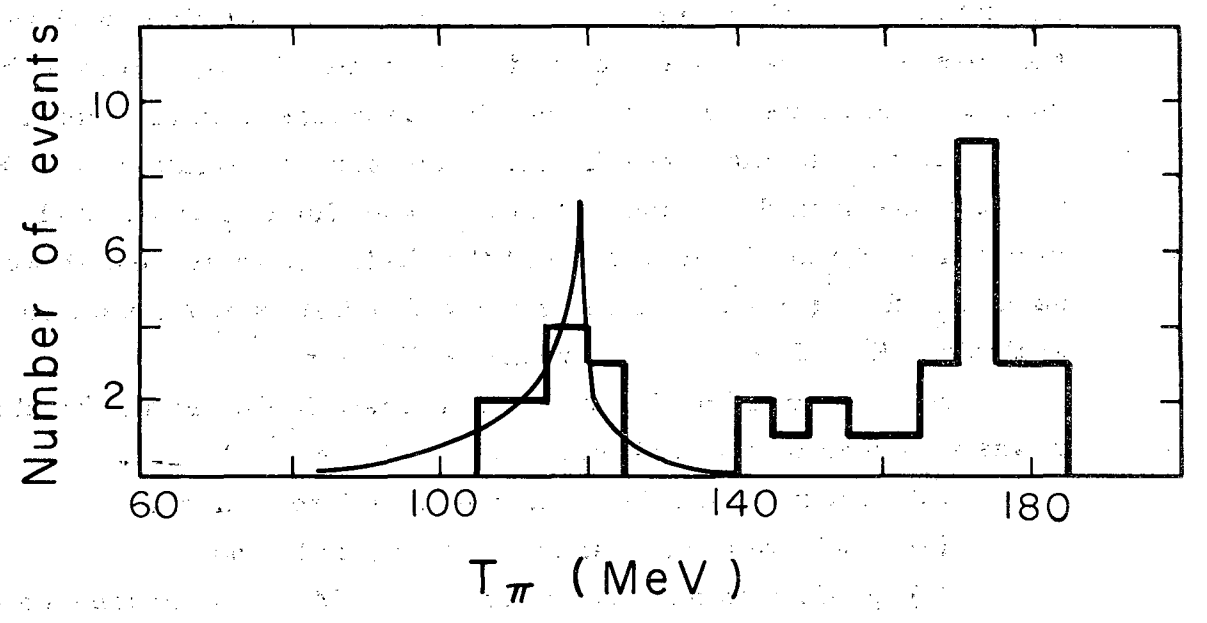

MU-27475

Fig. 8. Histogram of the center-of-mass pion kinetic energy in the reaction $K^- + d \rightarrow \Lambda + \pi^- + p$. The curve is the predicted conversion spectrum for a Σ-N scattering length of (-1+i) fermis.

Thus, the 37 measured $\Lambda\pi^- p$ events can be divded into 22 impulse events (65%), 11 internal conversions (35%) and less than 2 Y_1^* events (less than 5%).

It is interesting to compare these ratios with the ratios at rest. We see that as the K^- energy is increased more events fit a simple impulse model. The Y_1^* production has decreased sharply, and the internal conversion has decreased somewhat but is still important. This is what we would expect on a naive basis. As the K^- momentum increases, the wavelength of the K^- meson becomes smaller and it tends to see the deuteron as simply a neutron and a proton.

The Y_1^* production will be expected to decrease because, as the incident-beam energy goes up, a higher-energy proton is required kinematically in Y_1^* production and the deuteron-wave function does not contain a large high-energy component.

C. The Reactions $K^- + d \rightarrow \Sigma + \pi + N$

In the reactions $K^- + d \rightarrow \Sigma + \pi + N$, we can calculate all the physical variables for four final states.

They are

$$K^- + d \rightarrow \begin{cases} \Sigma^0 + \pi^- + p, \\ \Sigma^- + \pi^0 + p, \\ \Sigma^- + \pi^+ + n, \text{ and} \\ \Sigma^+ + \pi^- + n. \end{cases}$$

In all these final states the Dalitz plots (Figs. 10 through 13) are not uniformly populated; most of the events have low-energy nucleons.

The $\Sigma^0 \pi^- p$ and $\Sigma^- \pi^0 p$ final states seem to fit the impulse model well. In Figs. 14 and 15 we have plotted their proton-energy distribution in the laboratory system. The proton energy is known to approximately 2 MeV if the proton is visible. If the proton is not visible it is only known to have an energy less than 3 MeV. Within the limited statistics available, these two final states seem to be dominated

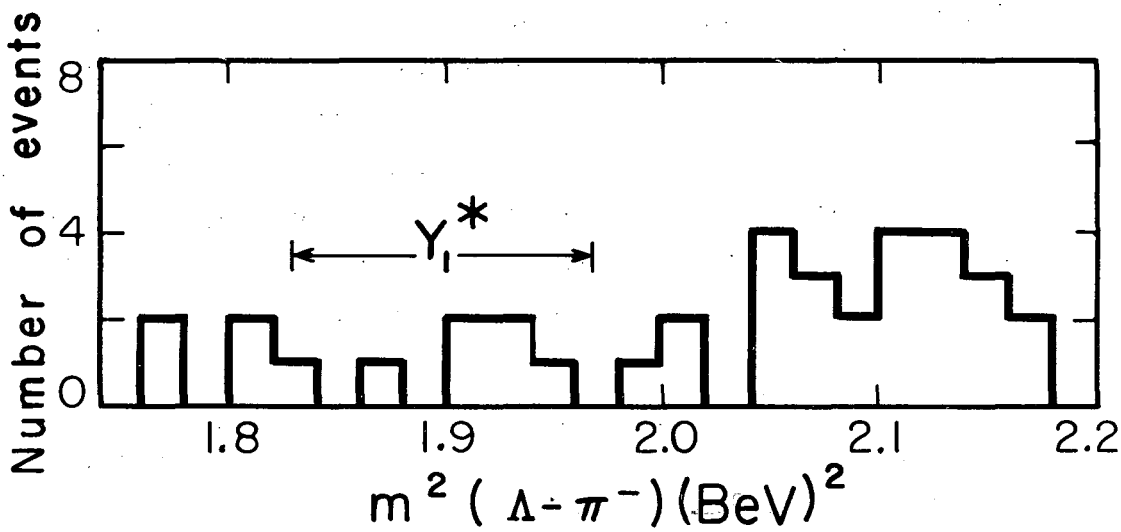

MU-27476

Fig. 9. Distribution of the square of the effective mass of the Λ-π system in the reaction $K^- + d \rightarrow \Lambda + \pi^- + p$.

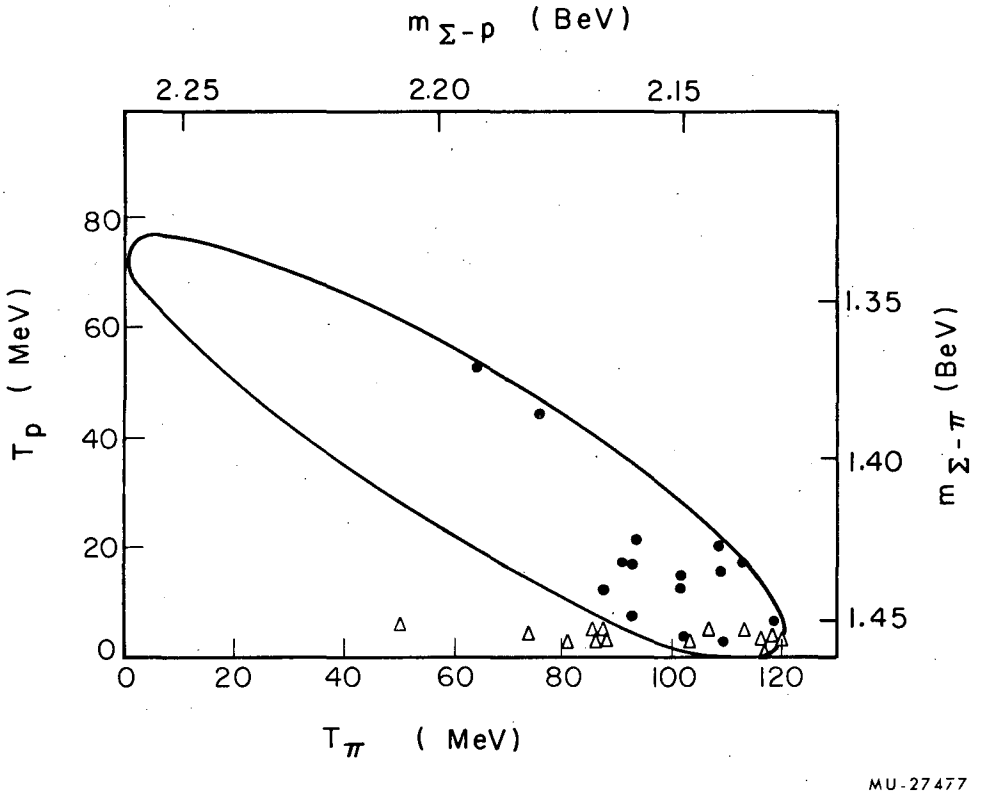

Fig. 10. Normalized Dalitz plot for the reaction $K^- + d \rightarrow \Sigma^0 + \pi^- + p$. The deltas represent events in which the proton track was not seen.

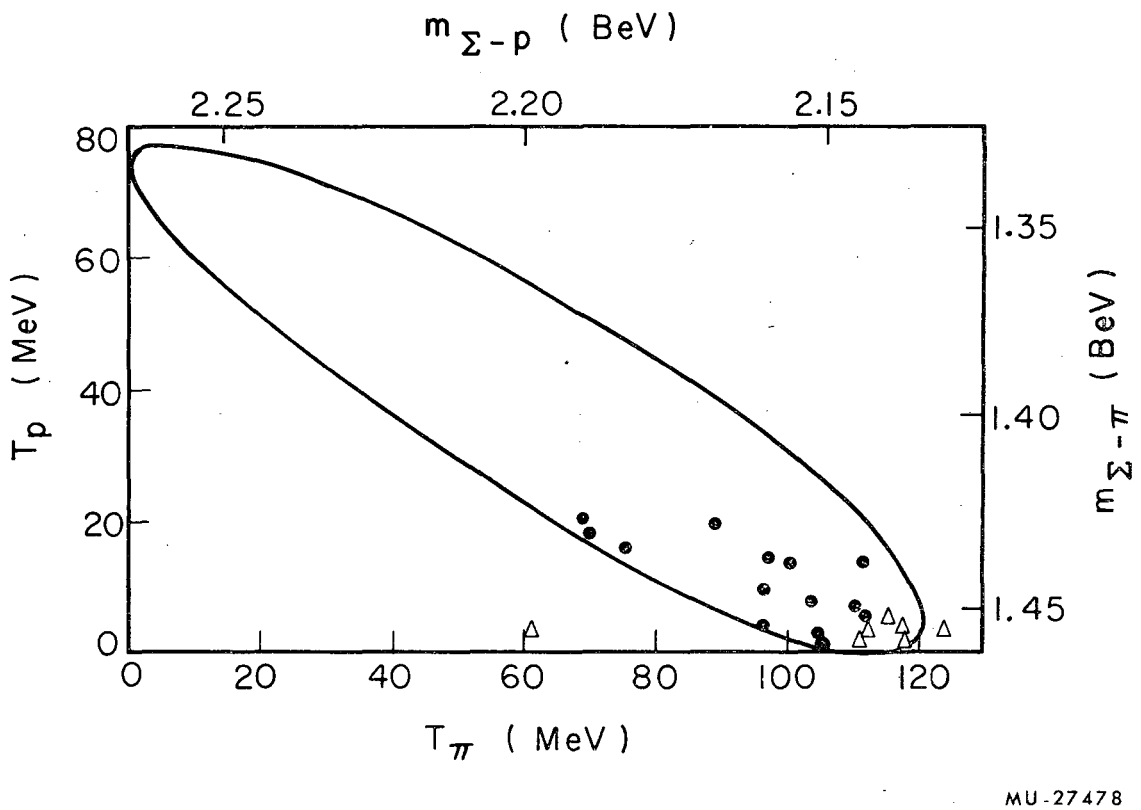

Fig. 11. Normalized Dalitz plot for the reaction $K^- + d \rightarrow \Sigma^- + \pi^0 + p$. The deltas represent events in which the proton track was not seen.

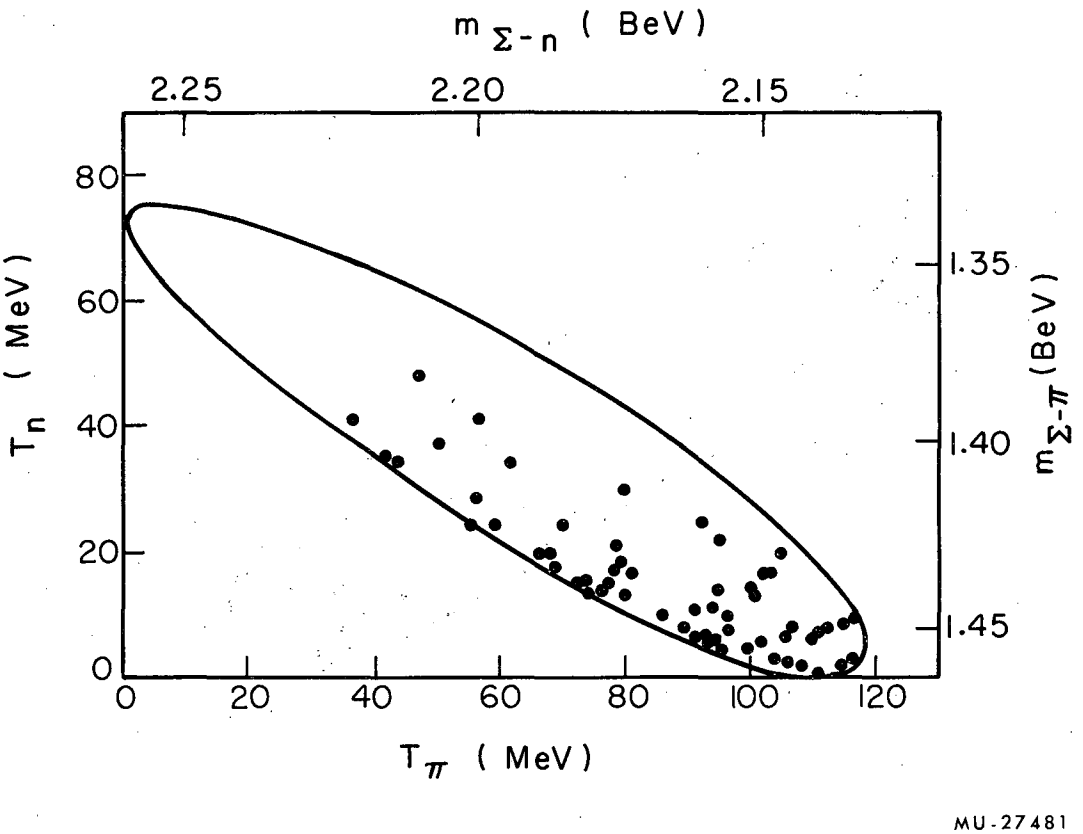

Fig. 12. Normalized Dalitz plot for the reaction $K^- + d \rightarrow \Sigma^+ + \pi^- + n$.

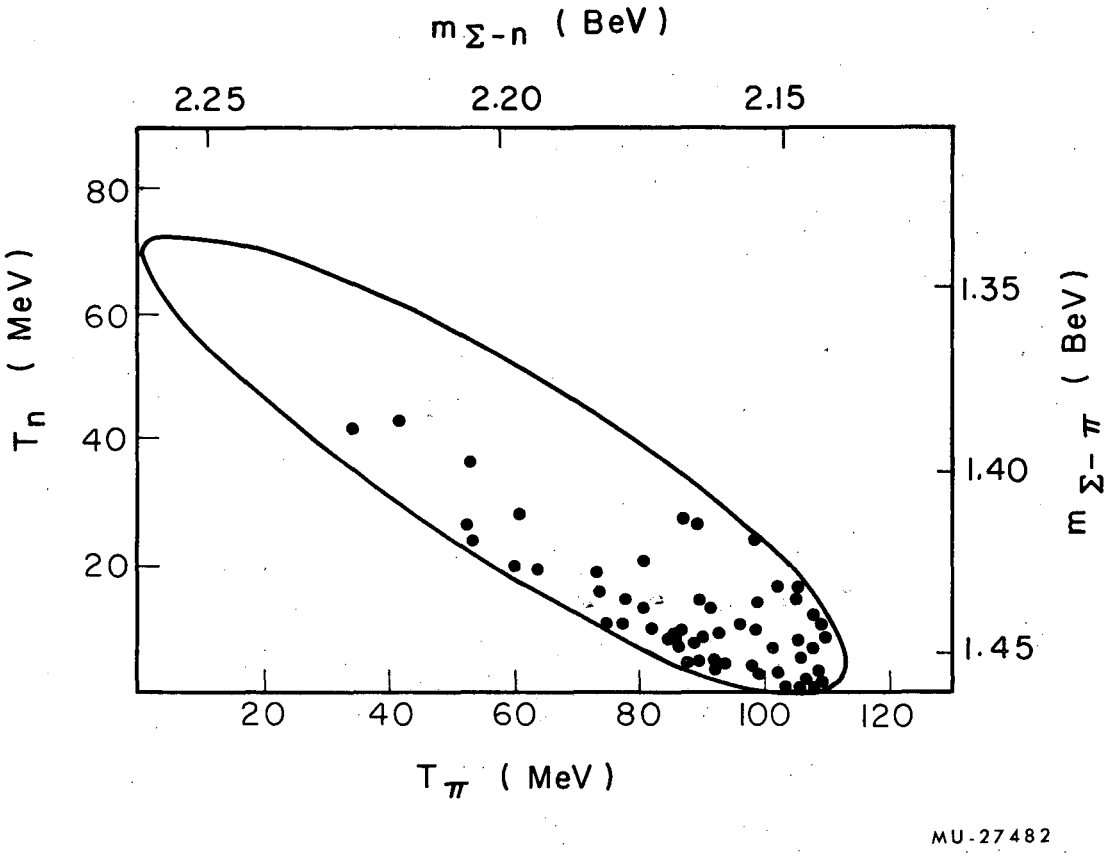

Fig. 13. Normalized Dalitz plot for the reaction $K^- + d \rightarrow \Sigma^- + \pi^+ + n$.

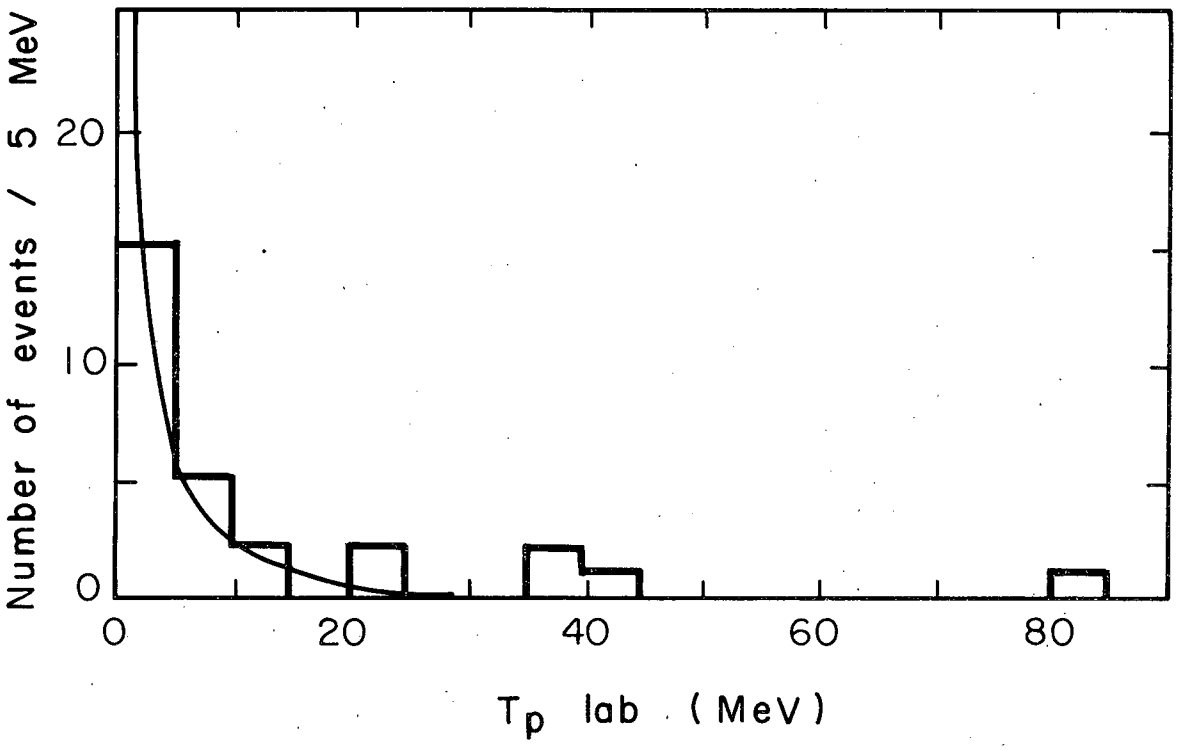

Fig. 14. Histogram of the laboratory-system kinetic energy of the proton in the reaction $K^- + d \rightarrow \Sigma^0 + \pi^- + p$. The curve is the prediction according to the impulse model.

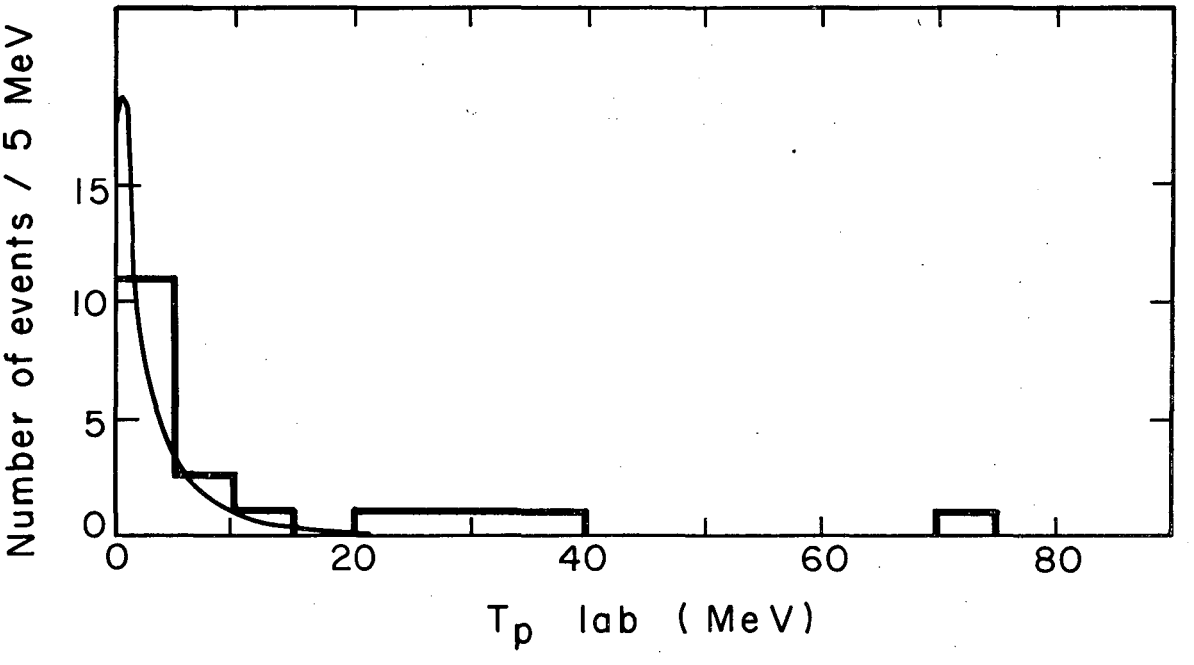

Fig. 15. Histogram of the laboratory-system kinetic energy of the proton in the reaction $K^- + d \rightarrow \Sigma^- + \pi^0 + p$. The curve is the prediction according to the impulse model.

by the impulse events. There are two or three events with high-energy protons that are presumably caused by final-state scattering, but the statistics are clearly too limited for us to attempt a more detailed analysis. We would expect some distortion of the spectra as a result of pion-nucleon scattering since the maximum pion-nucleon energy is only one half-width (38 MeV) below the peak of the first pion-nucleon resonance.

In the $\Sigma^-\pi^+n$ and $\Sigma^+\pi^-n$ final states the impulse model seems to have some effect but does not adequately explain the data as we can see in Figs. 16 and 17. In these two channels the neutron energy is known only within 5 to 10 MeV, and we would expect that the experimental distribution of neutron kinetic energies would be broadened. However, in the Dalitz plots we see that there are many events with pion energy too low to be impulse events, even if the neutron energy had been miscalculated. Some of these events, however, could be interactions at rest which form a 25 to 30% contamination in these measurements. The difference between these distributions and the $\Sigma^-\pi^0p$ and $\Sigma^0\pi^-p$ may be caused by the I = 0, 1405-MeV, $\Sigma\pi$ resonance recently reported.[12, 13, 14, 15] In the $\Sigma^-\pi^0p$ and $\Sigma^0\pi^-p$ final states the $\Sigma\pi$ system is in a pure I = 1 state. However, in the $\Sigma^-\pi^+n$ and $\Sigma^+\pi^-n$ the $\Sigma\pi$ system is a mixture of I = 0 and I = 1. Hence, we would expect the Y_0^* $\Sigma\pi$ resonance to have an effect on these two final states. In Figs. 18 and 19 we have plotted the square of the $\Sigma\pi$ effective mass for the $\Sigma^-\pi^+n$ and $\Sigma^+\pi^-n$ states. We see no evidence for a peaking of events at the Y_0^* mass. However, if the Y_0^* is a K^--nucleon bound-state resonance as suggested by Schult and Capps, it would not necessarily appear as a typical resonance bump; it may merely make the proton momentum distribution from the wave function broaden and become less peaked.[16] This broadening is approximately what we see in these two channels. However, the difficulty of eliminating the interactions at rest and the relatively poor energy resolution of the

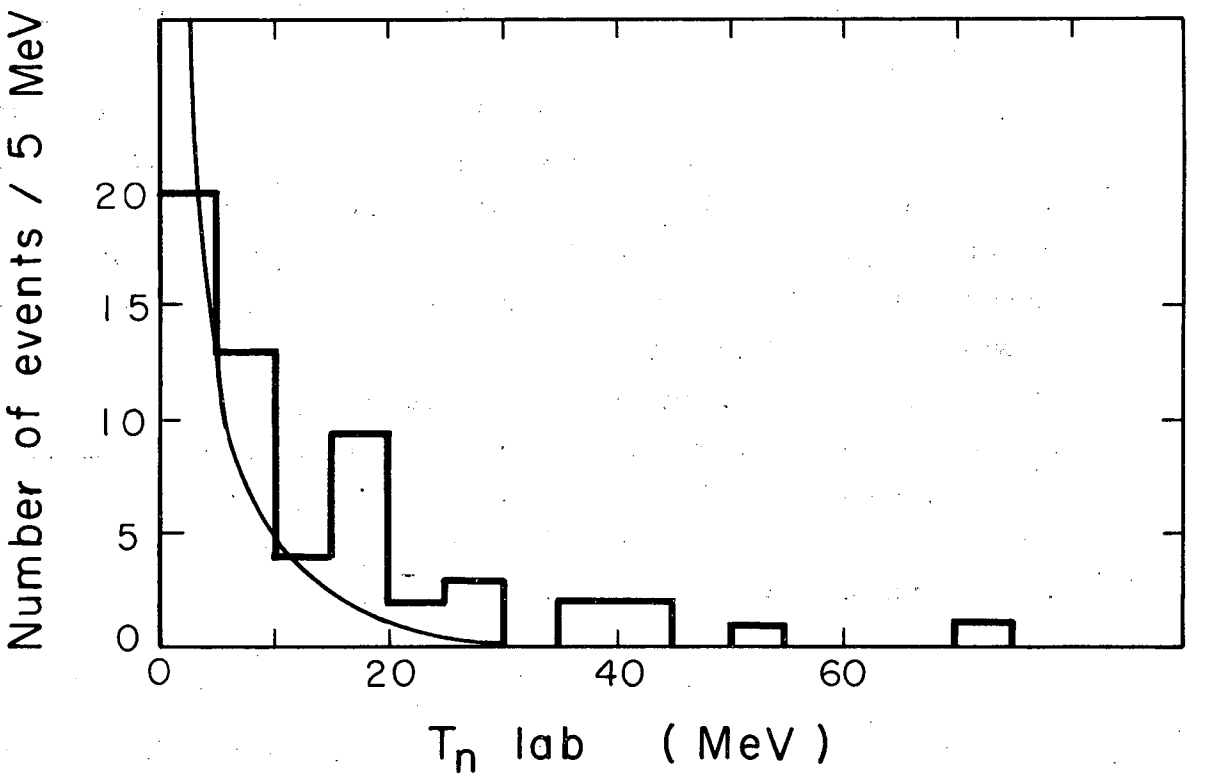

Fig. 16. Histogram of the laboratory-system kinetic energy of the neutron in the reaction $K^- + d \rightarrow \Sigma^- + \pi^+ + n$. The curve is the prediction according to the impulse model.

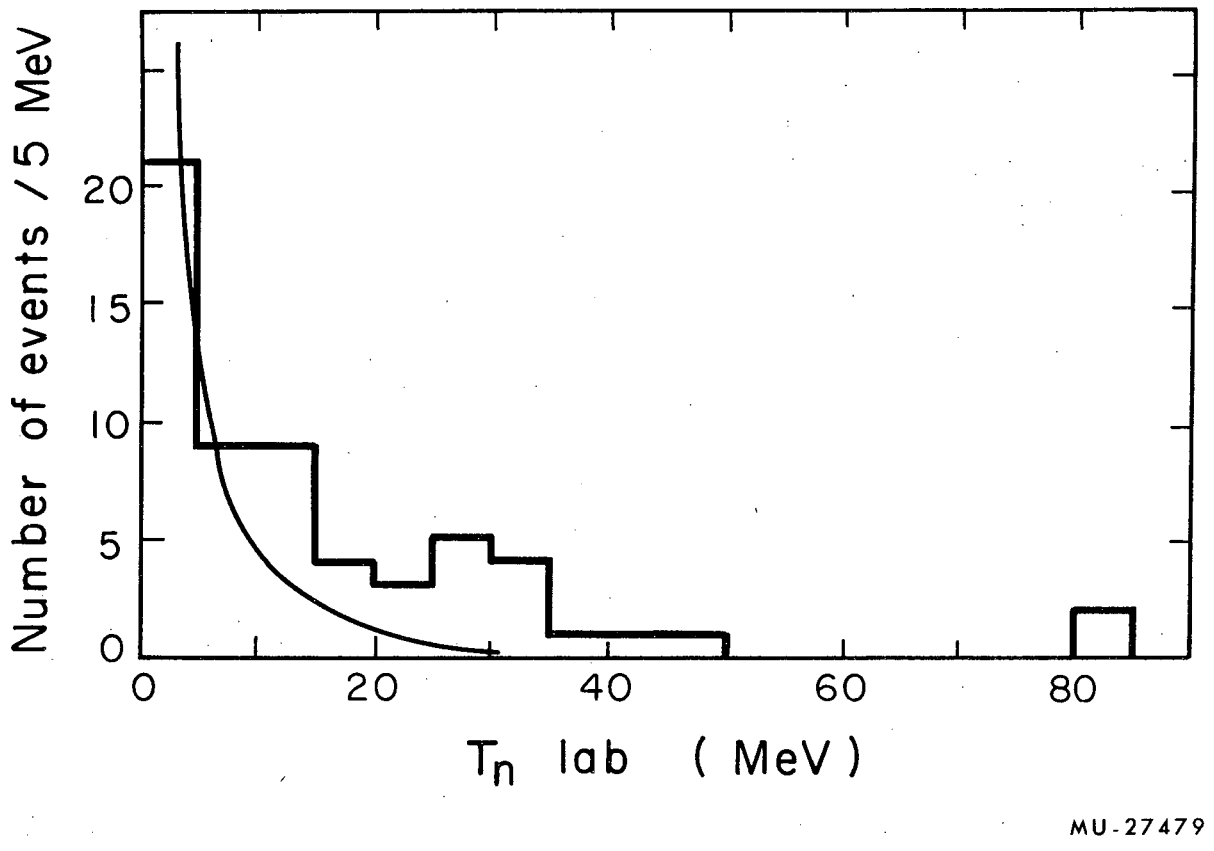

Fig. 17. Histogram of the laboratory-system kinetic energy of the neutron in the reaction $K^- + d \rightarrow \Sigma^+ + \pi^- + n$. The curve is the prediction according to the impulse model.

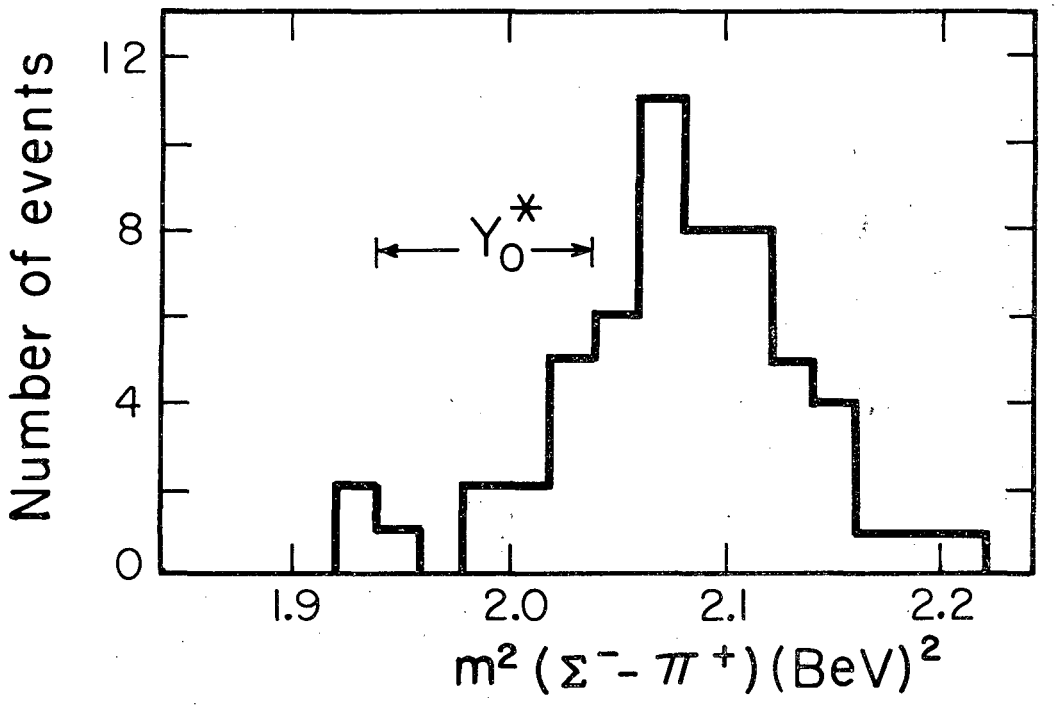

MU-27480

Fig. 18. Distribution of the square of the effective mass of the Σ-π system in the reaction $K^- + d \rightarrow \Sigma^- + \pi^+ + n$

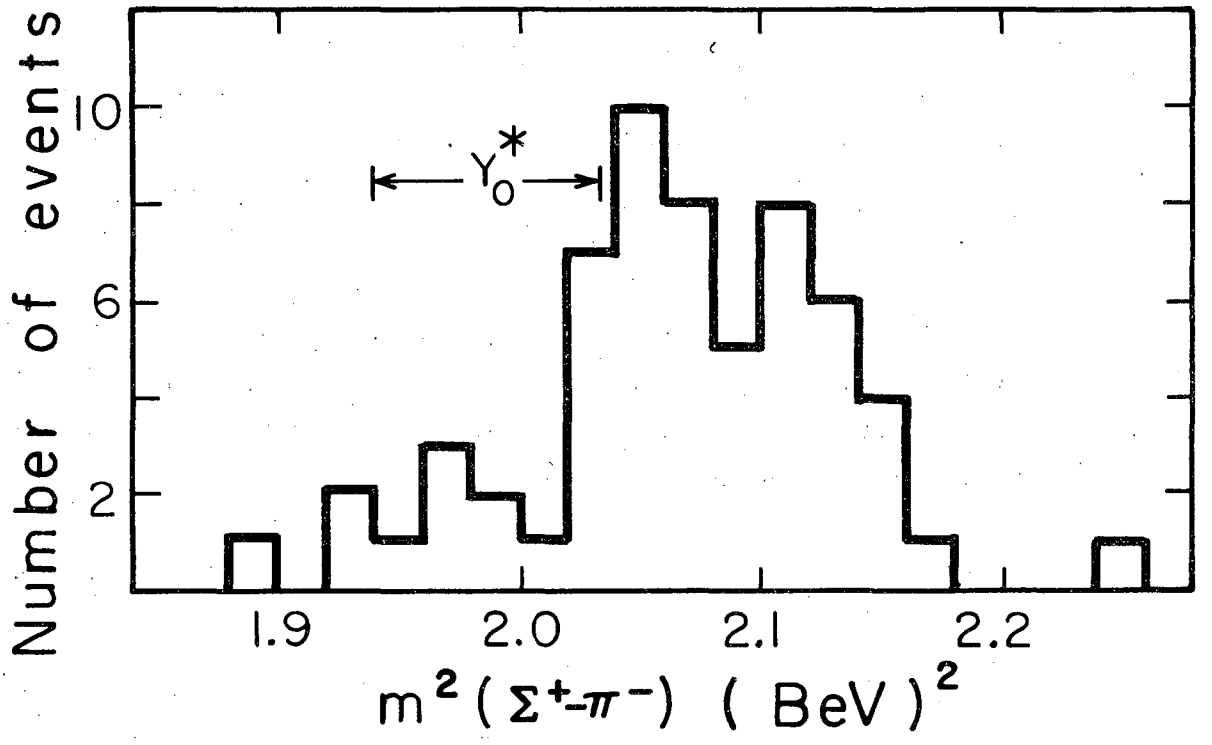

Fig. 19. Distribution of the square of the effective mass of the Σ-π system in the reaction $K^- + d \rightarrow \Sigma^+ + \pi^- + n$.

neutron make it impossible to decide whether the observed broadening is due to these effects or to the Y_0^* resonance.

D. The $\Sigma^0\pi^0 n$ and $\Lambda\pi^0 n$ Final States

Because, in the $\Sigma^0\pi^0 n$ and $\Lambda\pi^0 n$ final states, we cannot measure or calculate the physical variables of the π^0 or the neutron, we can only observe the kinetic-energy distribution of the Λ for both of these reactions together. In Fig. 20 we have plotted the kinetic-energy distribution for the Λ in the K^--d c.m. system. For comparison purposes Fig. 21 shows the kinetic-energy distribution in the production c.m. system for the Λ's from the $\Lambda\pi^- p$ final state and from the $\Sigma^0\pi^- p$ final state.

We have weighted the $\Lambda\pi^- p$ and $\Sigma^0\pi^- p$ final states so that the distributions contain 40 directly produced Λ's and 32 Λ's from Σ^0 decay, which is the number of $\Lambda\pi^0 n$ and $\Sigma^0\pi^0 n$ events predicted by the use of charge independence.

The energy distributions for the $\Lambda\pi^0 n$ and $\Sigma^0\pi^0 n$ final states show no significant difference from the comparison distribution from $\Lambda\pi^- p$ and $\Sigma^0\pi^- p$.

E. Nonmesonic Final States

The outstanding feature of the two-body final states is their branching ratio; only 2% of the hyperon production occurs in these modes. This is quite surprising on energetic grounds since the two-body final state has 140 MeV more energy available than the three-body state. However, it is readily understandable when we consider the loose structure of the deuteron. To produce a two-body final state the K^- meson has to interact with both the proton and the neutron together and because the deuteron is diffuse this is unlikely. However, to produce a three-body final state the K^- need interact with only one nucleon.

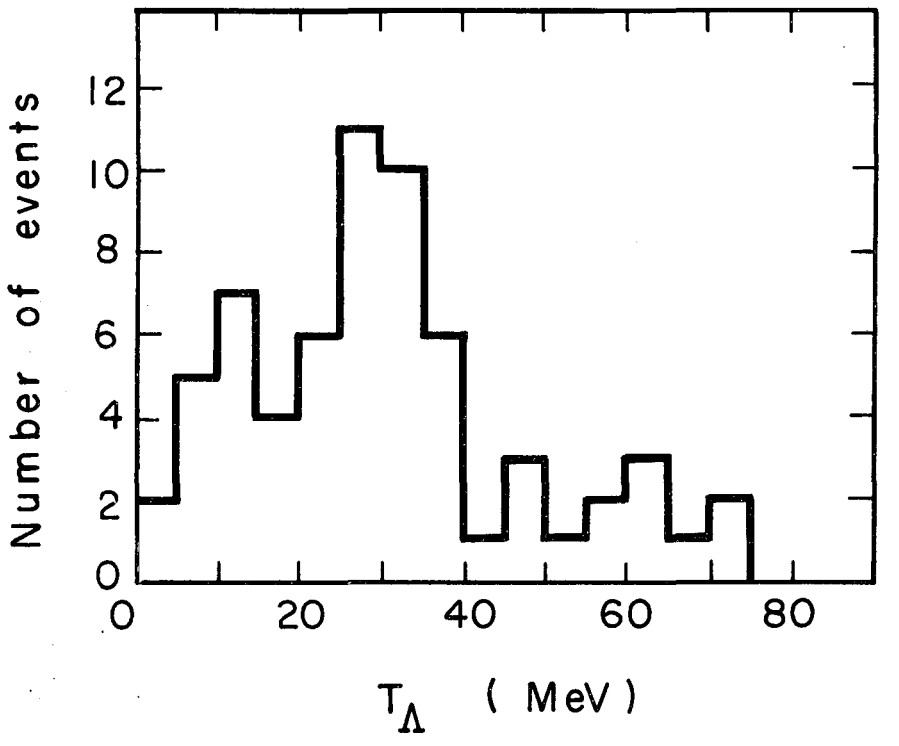

Fig. 20. Histogram of the kinetic energy of the Λ in the K^-d c.m. system for the reactions $K^- + d \rightarrow \Sigma^0 + \pi^0 + n$ and $K^- + d \rightarrow \Lambda + \pi^0 + n$.

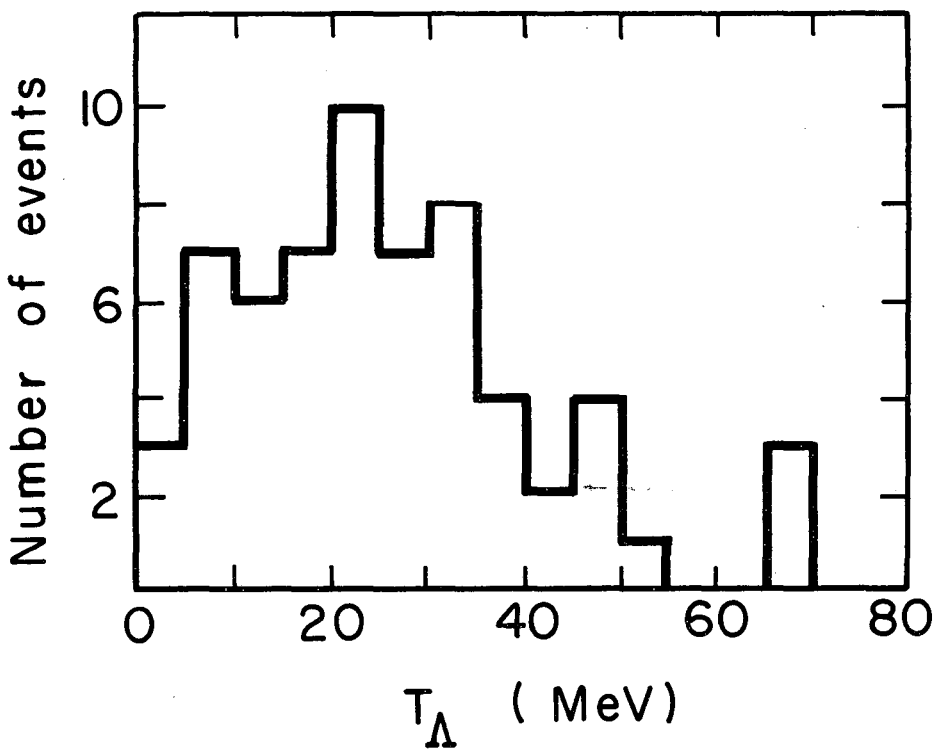

MU-27488

Fig. 21. Histogram of the Λ kinetic energy in the K^-d c.m. system for the reaction $K^- + d \rightarrow \Lambda + \pi^- + p$ and $K^- + d \rightarrow \Sigma^0 + \pi^- + p$, followed by $\Sigma^0 \rightarrow \Lambda + \gamma$. The ratios have been normalized to give the same Σ/Λ ratio as is predicted by charge independence for $K^- + d \rightarrow \Sigma^0 + \pi^0 + n$ and $K^- + d \rightarrow \Lambda + \pi^0 + n$.

F. Comparison Between K^-d and K^-p Interactions

It is interesting to analyze our branching ratios in terms of the K^-p interactions. Recently, Humphrey and Ross[17] have carefully studied the low-energy K^-p system by using the zero-effective-range formalism of Dalitz and Tuan.[18] They find two solutions which predict practically identical branching ratios for K^-d above 150 MeV/c laboratory-system momentum. Since we wish to compare the K^-p and K^-d cross section at the same K-nucleon total energy, we compare results with the same incident energy in the laboratory system.

Because the branching ratios predicted by the two solutions are essentially identical, in making the comparison we shall use solution I of Hymphrey and Ross, which they consider to be the more probable one.

We may divide the deuterium interactions into two groups, those made on the proton and those made on the neutron.

The contribution to the cross section from the events on the proton we assume to be the same as the K^-p cross section. To calculate the K^--n part of the deuterium cross section we use Humphrey and Ross's estimate of the $I = 1$ cross section and their estimate of the fraction of Λ's produced in the $I = 1$ channel.

We calculate that the predicted cross section is σ (hyperon) = 116 mb.

We calculated branching ratios are listed in Table V.

Agreement between the calculated and measured values is quite good. The agreement of the total cross sections to within 1.5 mb is obviously fortuitous, since Humphrey and Ross find that the K^-p cross sections are varying rapidly in this energy region and the cross section measured in this experiment is an average over a comparitively large momentum interval.

This direct comparison, however, neglects the Σ-Λ conversion process. Lambdas produced in this way are really associated with the initial production of Σ's.

The final-state interaction mixes the Σ-Λ system so that a comparison between all seven states is no longer meaningful. However, as Schult and Capps have pointed out, we may still compare the ratios of the Σ-N isotopic-spin states.[16]

Table V. K^-d rates calculated from solution I (P_K=187.5 MeV/c) of Humphrey and Ross.[17]

Final state	K^-d rates calculated from solution I	
	Cross section	Branching ratio
$\Sigma^- \pi^+ n$	20.4	0.176
$\Sigma^+ \pi^- n$	22.4	0.195
$\Sigma^0 \pi^0 n$	13.8	0.120
$\Lambda \pi^0 n$	10.1	0.087
$\Sigma^- \pi^0 p$	14.8	0.127
$\Sigma^0 \pi^- p$	14.8	0.127
$\Lambda \pi^- p$	19.8	0.171
all hyperons	116.1	1.00

Experimentally we get, for the ratios (using the results that have been fitted to charge independence),

$$W_{\frac{3}{2}} / W_{\frac{1}{2}} / W_{\Lambda} = 0.24/0.55/0.21$$

whereas the K^-p data give

$$W_{\frac{3}{2}}/W_{\frac{1}{2}}/W_{\Lambda} = 0.39/0.42/0.19.$$

Here

$W_{\frac{3}{2}}$ = initial Σ production with the Σ-N in an $I = 3/2$ state,

$W_{\frac{1}{2}}$ = initial Σ production with the Σ-N in an $I = 1/2$ state,

W_{Λ} = direct Λ-N production.

The agreement between the predicted and experimental values is excellent for W_{Λ}. The disagreement between the experimental and predicted values for $W_{\frac{3}{2}}$ and $W_{\frac{1}{2}}$ should not be taken very seriously because of the effect of pion-nucleon scattering. At an incident laboratory-spectrum momentum of 200 MeV/c the maximum pion-nucleon energy is only one half-width (38 MeV) below the peak of the first pion-nucleon resonance. The resulting pion-nucleon scattering in the $I = 3/2$ state changes the ratio of $W_{\frac{3}{2}}$ and $W_{\frac{1}{2}}$.

We may also directly calculate the ratio

$$\epsilon = \left. \frac{KN \rightarrow \Lambda\pi}{(KN \rightarrow \Lambda\pi)+(KN \rightarrow \Sigma\pi)} \right|_{I=1}$$

which is the fraction of the $I = 1$ K^-p absorption that produces Λ's.

To calculate this we look at impulse events in the reactions

$$K^- + d \rightarrow \Sigma^0 + \pi^- + p,$$

and

$$K^- + d \rightarrow \Lambda + \pi^- + p,$$

and use charge independence to estimate the total number of $\Sigma\pi$ events;

$$(K^- + n \rightarrow \Sigma + \pi) = 2\ (K^- + n \rightarrow \Sigma^0 + \pi^-).$$

We consider an event to be an impulse-type event if the proton track is not visible. Thus, since these two reactions look the same on the scanning table and we are selecting impulse events by the same visual criterion, we have no bias caused by different scanning efficiencies or by the idiosyncrasies of the kinematic fitting.

In our data we have 13 $\Lambda\pi^-p$ and 14 $\Sigma^0\pi^-p$ events that fit the impulse model. This yields the value

$$\epsilon = 0.32 \pm 0.08 .$$

The value of ϵ is slightly lower than the value of 0.40 found by Humphrey and Ross in K^-p interactions at rest, and is in excellent agreement with the value of 0.33 ± 0.14 found by Luers et al.[19] in $K_2^0 + p$ interactions at 230 MeV/c.

ACKNOWLEDGMENTS

In any experiment involving the use of equipment such as the Bevatron, the 15-inch bubble chamber, and the 7090 computer, the time and effort of many people are required. It is with pleasure that I acknowledge the aid and support of Professor Luis Alvarez and the invaluable guidance of Professor Donald H. Miller. I would also like to thank Dr. Joseph J. Murray, who supervised the design and construction of the beam. I am indebted to Professor Arthur H. Rosenfeld for many helpful discussions.

I also wish to express my appreciation to many scanners and technicians, in particular Mr. Larry Epperson and Mr. Robert Greaves.

This work was done under the auspices of the U. S. Atomic Energy Commission.

APPENDICES

A. Study of Uncertainties in the Observed Variables

To examine our fitting procedure we analyzed in detail the fits of 348 Λ decays. Since these decays can be unambiguously identified on the scanning table, we have no bias from incorrect hypotheses. In these events we can measure everything except for the momentum of the Λ. Hence, the decays have three constraints and we expect the mean value of χ^2 to be 3.

In Fig. 22 we have plotted the χ^2 distribution of the decays. The solid curve is the theoretical distribution; the experimental distribution has approximately the same shape but is about twice as broad. The dotted curve shows the expected distribution when we multiply the value of χ^2 by 1.8.

We also examined the "pull" quantities for the same events.[20] They are defined as

$$\xi_i = \frac{x_i^* - x_i^{meas.}}{\sqrt{(x_i^* - x_i^{meas.})^2}} ,$$

where x_i^* is the adjusted value corresponding to x_i^{meas}.

If the values and errors are properly adjusted, the pull quantities should have a mean of zero and a width of one. The distributions are plotted in Figs. 23 through 26.

These distributions are too wide by a factor of 1.3. These plots and our χ^2 distribution indicate that we underestimated our errors by 30%. Hence, in analyzing our data, we scaled all χ^2's by a factor of 1.8 and multiplied all our estimated errors by 1.3. This procedure has no effect on the physical results.

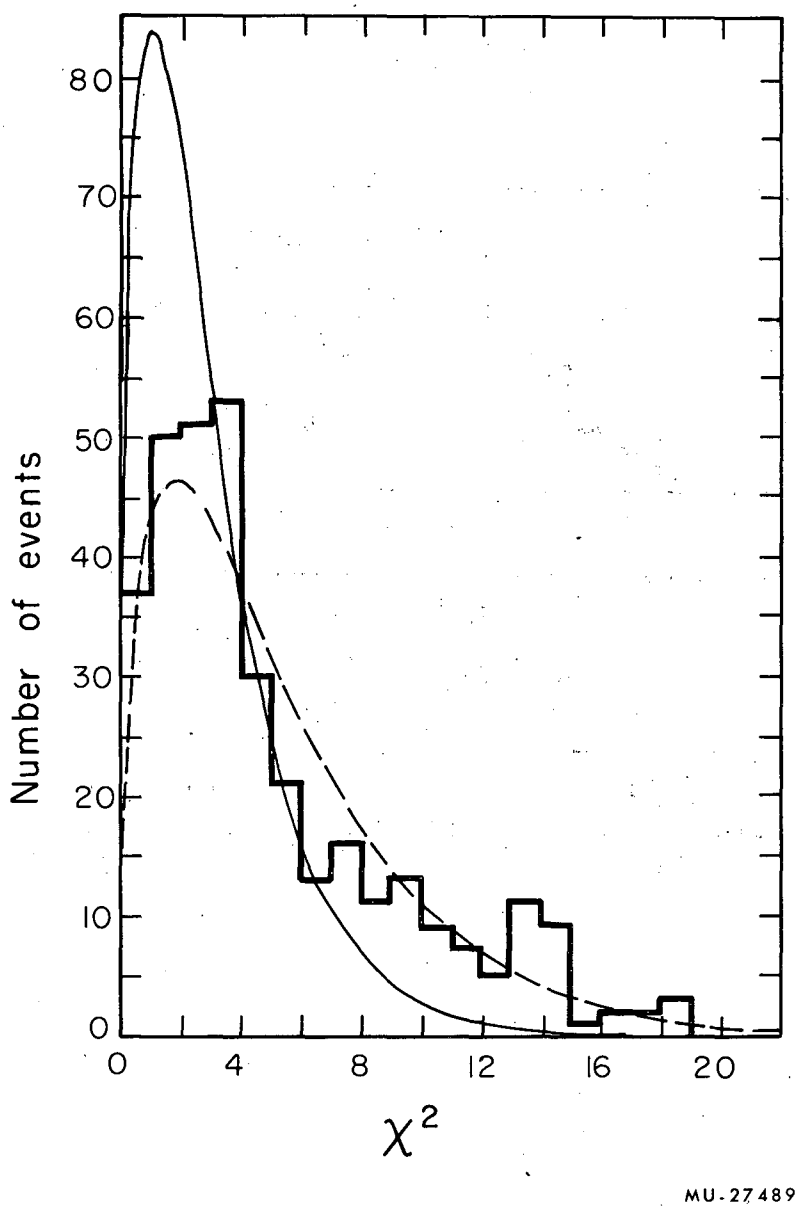

Fig. 22. Chi-square distribution for 347 Λ decays. The solid curve is the theoretical distribution and the dotted curve is the distribution with the absicca multiplied by 1.8

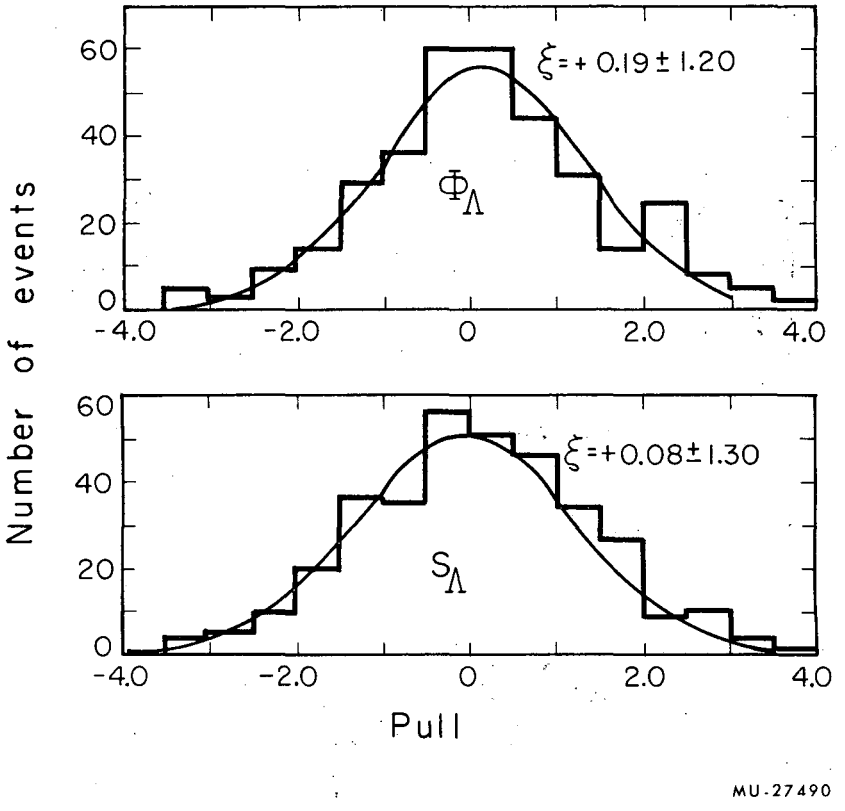

Fig. 23. "Pull" quantities for the Λ measurements in 347 Λ^- decays.

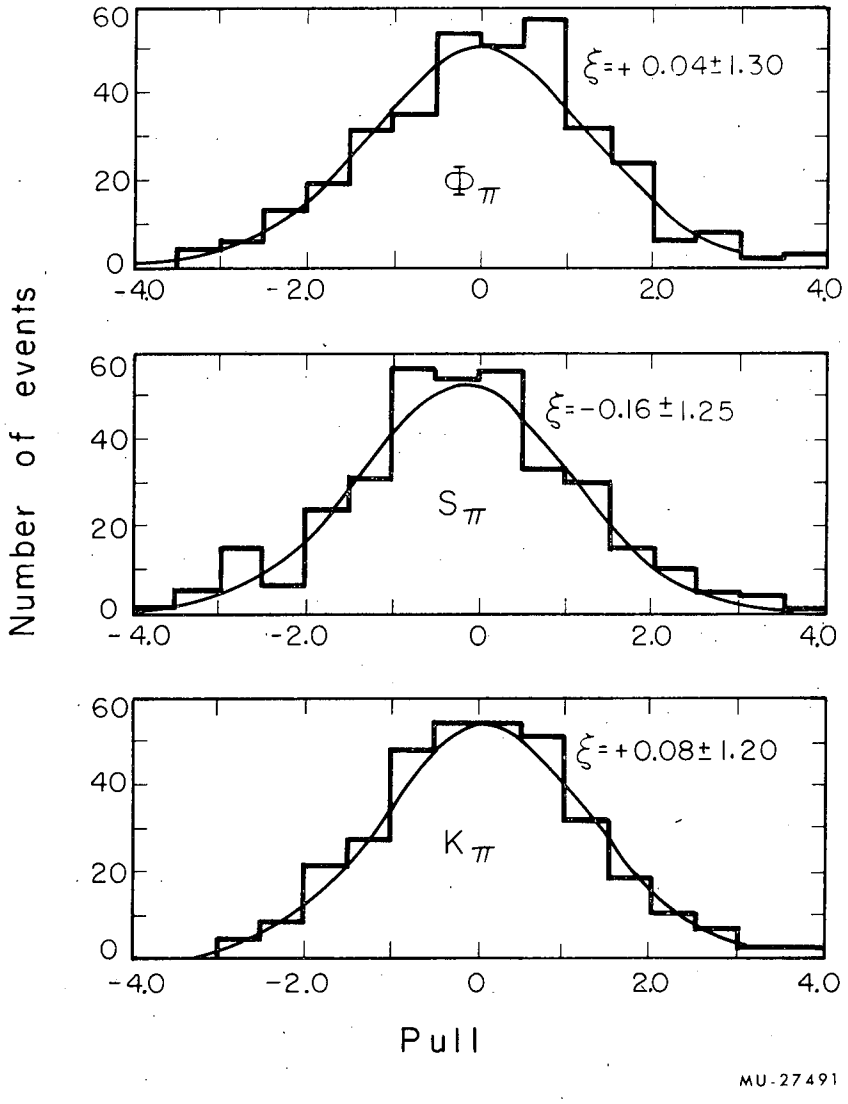

Fig. 24. "Pull" quantities for the π^- measurements in 347 Λ decays.

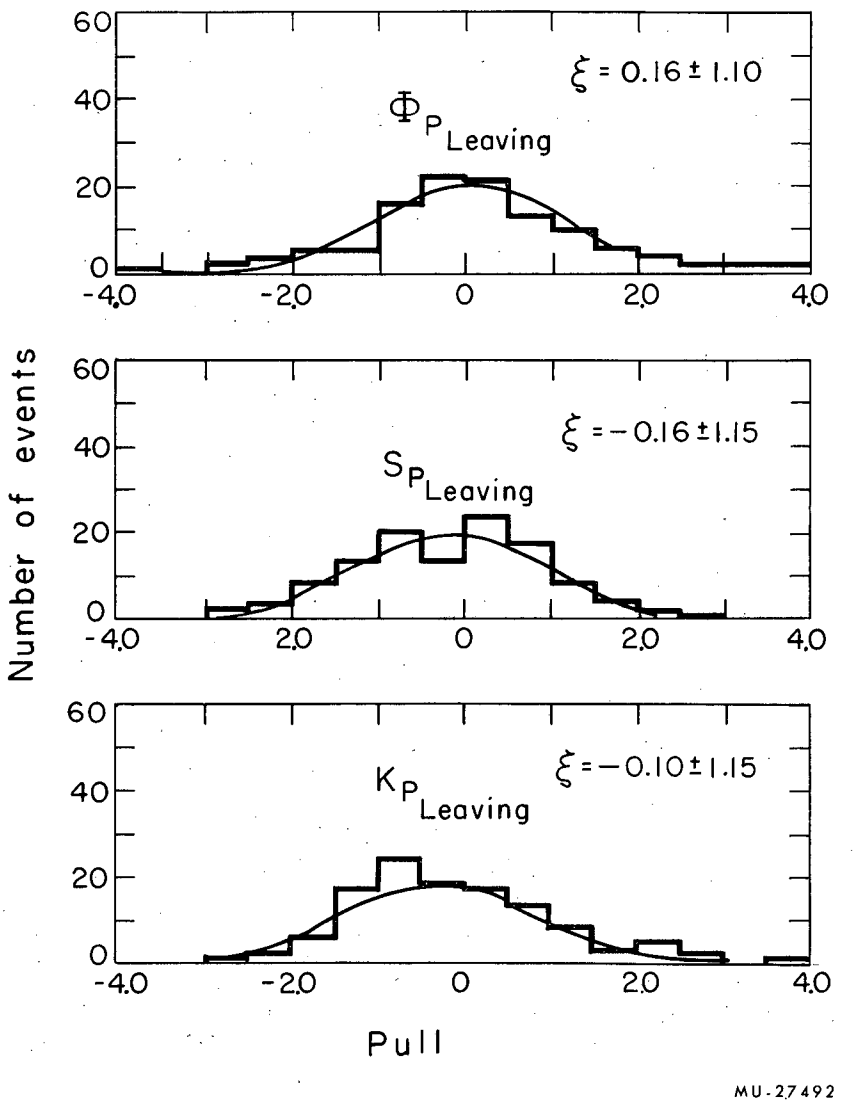

Fig. 25. "Pull" quantities for 114 nonstopping protons from Λ decays.

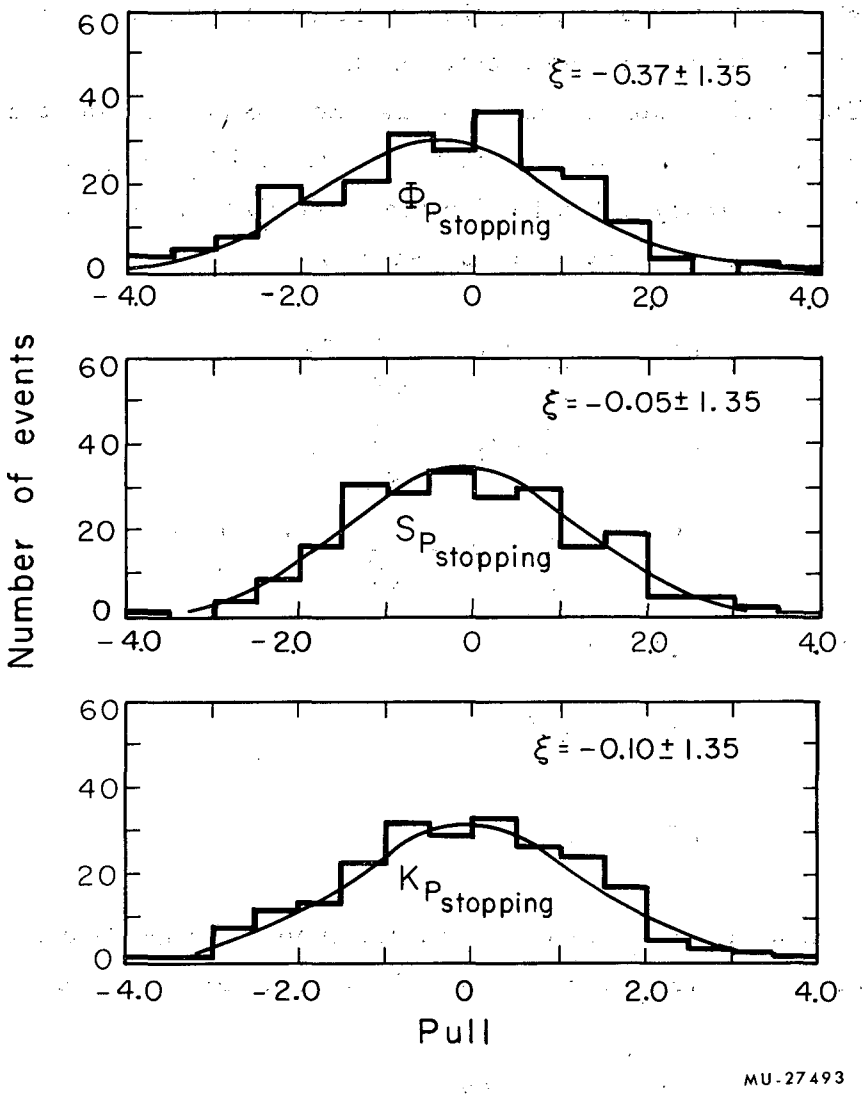

Fig. 26. "Pull" quantities for 233 stopping protons from Λ decays.

B. Derivation of Charge-Independence Relations

For completeness, we reproduce the derivation of the matrix elements for the reactions $K^- + d \rightarrow \pi + Y + N$ that are listed in Table V.

We use two subscripts; the upper one represents the total I spin and the lower one the z component.

The initial state is easy to analyze. Since the deuteron has $I = 0$, the initial state must be pure $I = 1/2$ and $I_z = -1/2$.

Now we analyze the final state. We first consider the pion-hyperon system. We have the $\Sigma\pi$ system

$$\psi_0^1 = \frac{1}{\sqrt{2}} \Sigma^+ \pi^- - \frac{1}{\sqrt{2}} \Sigma^- \pi^+ ,$$

$$\psi_{-1}^1 = \frac{1}{\sqrt{2}} \Sigma^0 \pi^- - \frac{1}{\sqrt{2}} \Sigma^- \pi^0 ,$$

and

$$\psi_0^0 = \frac{1}{\sqrt{3}} \Sigma^+ \pi^- - \frac{1}{\sqrt{3}} \Sigma^0 \pi^0 + \frac{1}{\sqrt{3}} \Sigma^- \pi^+ ,$$

and for the $\Lambda\pi$ system

$$\phi_0^1 = \Lambda \pi^0 ,$$

and

$$\phi_1^1 = \Lambda \pi^- .$$

We now combine these states with a nucleon. We get two independent wave functions which have $I = 1/2$, $I_z = -1/2$ for Σ's and one for Λ's. They are

$$\frac{1}{\sqrt{3}} \psi_0^1 \; n - \sqrt{\frac{2}{3}} \psi_{-1}^1 \; p$$

$$\psi_0^0 \; n$$

$$\frac{1}{\sqrt{3}} \phi_0^1 \; n - \sqrt{\frac{2}{3}} \phi_{-1}^1 \; p$$

We can also get other wave functions with $I = 3/2$ or $I = 5/2$. Everything so far is formal; we can describe any system in terms of states of definite isotopic spin.

Charge independence, however, states that the interaction must conserve isotopic spin. Thus, the foregoing three states are the only allowed ones and we may write the final state as

$$M_1\left(\sqrt{\tfrac{1}{3}}\psi_0^1\ n - \sqrt{\tfrac{2}{3}}\psi_{-1}^1\ p\right) + M_0\psi_0^0\ n + M_\Lambda\left(\sqrt{\tfrac{1}{3}}\phi_0^1\ n - \sqrt{\tfrac{2}{3}}\phi_0^1\ n - \sqrt{\tfrac{2}{3}}\phi_{-1}^1\ p\right).$$

We then re-express this in terms of charge states, and square to get the rates listed in Table V.

REFERENCES

1. Pierre Bastien, Orin Dahl, Joseph Murray, Mason Watson, R. G. Ammar, and Peter Schlein, in Proceedings of the International Conference on Instrumentation for High Energy Physics, Berkeley, 1960 (Interscience Publishers, Inc., New York, 1960), pp 299-301.
2. Joseph J. Murray, in Proceedings of an International Conference on Instrumentation for High Energy Physics, Berkeley, 1960 (Interscience Publishers, Inc., New York, 1961), pp 25-33.
3. Arthur H. Rosenfeld, in Proceedings of the International Conference on High Energy Accelerators and Instrumentation (CERN Scientific Information Service, Geneva, 1959), pp 533-541. Also, W. E. Humphrey, "A Description of the PANG Program", Alvarez Group Memorandum No. 111 and No. 115, Lawrence Radiation Laboratory (unpublished).
4. Arthur H. Rosenfeld and James N. Snyder, Rev. Sci. Instr. 33, 181 (1962).
5. Luis W. Alvarez, in Ninth International Annual Conference on High Energy Physics (Moscow, 1960), pp 471 to 526.
6. Glenwood Clark Jr., and William F. Diehl, Range-Energy Relation for Liquid-Hydrogen Bubble Chambers (M. S. Thesis), University of California Radiation Laboratory Report UCRL-3789, May 1957 (unpublished).
7. Gerson Goldhaber and Sulamith Goldhaber (Lawrence Radiation Laboratory), private communication.
8. R. H. Dalitz, Phys. Rev. 94, 1946 (1954).
9. Robert Karplus and Leonard S. Rodberg, Phys. Rev. 115, 1058 (1959).
10. T. Kotani and M. Ross, Nuovo cimento 14, 1282 (1959).
11. O. Dahl, N. Horwitz, D. H. Miller, J. J. Murray, and P. G. White, Phys. Rev. Letters 6, 142 (1961).

12. M. H. Alston, L. W. Alvarez, P. Eberhard, M. L. Good, W. Graziano, H. K. Ticho, and S. G. Wojcicki, Phys. Rev. Letters 6, 699 (1961).
13. P. Bastien, M. Ferro-Luzzi, and A. H. Rosenfeld, Phys. Rev. Letters 6, 702 (1961).
14. G. Alexander, G. R. Kalbfleisch, D. H. Miller, and G. A. Smith, Phys. Rev. Letters 8, 447 (1962).
15. M. H. Alston, L. W. Alvarez, M. Ferro-Luzzi, A. H. Rosenfeld, H. K. Ticho, S. G. Wojcicki, Study of Resonances in the Σ-π System, 1962 International Conference on High Energy Physics at CERN (to be published).
16. R. L. Schult and R. H. Capps, Phys. Rev. 122, 1659 (1961).
17. W. E. Humphrey and R. R. Ross, Low-Energy Interactions of K^- Mesons in Hydrogen, Phys. Rev. (to be published).
18. R. H. Dalitz and S. F. Tuan, Ann. Phys. 10, 307 (1960).
19. D. Luers, I. S. Mittra, W. J. Willis, S. S. Yamamoto, Phys. Rev. Letters 7, 255 (1961).
20. J. P. Berge, F. T. Solmitz, and H. Taft, Rev. Sci. Instr. 32, 538 (1961).